Universitetet i Stavanger

FACULTY OF SCIENCE AND TECHNOLOGY

MASTER'S THESIS

Study programme / specialisation: Master of Science Structural Engineering	**Spring 2023** Open / ~~Confidential~~
Author: Per Kristian Moi	
Supervisor(s) at UiS: Fredrik Bjørheim, Sudath C. Siriwardane **External supervisor:** Skar Tormod Barland	
Thesis title: Integrity Assessment of Mechanical Properties and Microstructure in Aging Railway Bridge in Norway	
Credits (ECTS): 30	
Keywords: *Railway bridge* *Old steel* *Mechanical testing* *Microstructure* *Lateral-torsional buckling*	Number of pages: 50 + appendix: 21 Stavanger, *05.07.2023*

Approved by the Dean 30 Sep 21

Faculty of Science and Technology

Acknowledgement

I am deeply grateful to my supervisors, Fredrik Bjørheim and Sudath C. Siriwardane, for their guidance and support throughout the development of this thesis. I would also like to extend my sincere appreciation to Johan Andreas Håland Thorkaas, whose invaluable advice, particularly during the stages of sample preparation and testing, significantly contributed to this work.

I am grateful for the support from everyone involved at UiS, with a special acknowledgment to the mechanical workshop team for their unwavering support and assistance.

Lastly, my thanks go to my external supervisor, Skar Tormod Barland from Bane NOR, whose contribution in supplying the old bridge material was crucial to the completion of this study.

Per Kristian Moi

Stavanger, June 2023

Abstract

There is a lack of documentation about the material in century-old railway bridges in Norway, with many of which are still in operation, approaching what is conventionally deemed as their design working life. Along with the ever-changing demands on the infrastructure, there is a growing concern regarding the remaining service life of these bridges and their capacity to accommodate modern traffic loads. To answer these questions, knowledge concerning the material and microstructural properties are essential.

This thesis aims to answer those questions by investigating the material composition and mechanical properties of a railway bridge of steel built in 1908 in Norway. The aim is to compare these findings with current steel standards and align the results with existing studies to enrich the understanding of their unique characteristics. This investigation involved a series of tests on the structure's four beams, one of them were used to extract specimen samples from, while the remaining three underwent buckling tests. Other testing included tensile, charpy impact, and hardness examination to determine mechanical properties. Spectroscopy were used to determine the chemical composition of a beam (Beam 2). Microstructure was assessed using light optical microscopy (LOM) and scanning electron microscopy (SEM). SEM was employed to gain insights into the fracture mechanisms, while energy-dispersive x-ray spectroscopy (EDS) was utilized to analyze the composition of non-metallic inclusions.

The results derived from these microstructural and mechanical assessments were then contrasted with those of prevalent structural steel alloy like S235, but also compared with those properties reported in literature of materials from same period. The study also explored potential enhancements to the bridge's strength via welding methods and compared theoretical and experimental buckling values.

As an exploratory study, this thesis aims to enrich the current understanding of century-old railway bridges in Norway by providing comprehensive data on the materials used in their construction. The research is intended as a pilot project to the analysis of other similar early 20^{th}-century bridges. The findings could not only form a basis for the development of precise evaluation techniques, but could also impact strategic decision-making regarding the safe, economical, and environmentally responsible preservation of these historic structures.

Table of content

List of Figures

List of Tables

1. Introduction

1.1 Context and background

At the turn of the 19th and 20th century, transportation systems experienced a significant evolution, with a substantial number of riveted steel bridges constructed across various countries. As these structures approach well over 100 years, they simultaneously approach what is conventionally deemed as their design working life – a concept not factored into account for when originally built. Despite enduring the tests of time, their continued suitability necessitates a reevaluation, especially in light of new standards and requirements. Various factors might necessitate a safety evaluation of these existing railway bridges. These include the need to carry heavy loads that is beyond initial limits, structural modifications as a result of deterioration, mechanical damage or repairs, changes in the bridge's function, or the need to comply with current standards and load requirements when repurposed for new railway links [1, 2].

To address these challenges, an integrity assessment is invaluable, a thorough evaluation of the bridge's current condition and performance based on current operational conditions. The aim is to pinpoint potential risks related to stability, strength, fatigue, and critical areas susceptible to unseen damage or cracks that could lead to bridge failure.

A significant hurdle in assessing the integrity of these century-old structures lies in the absence of necessary documentation or a complete and accurate depiction of these structures. The issue of "is the bridge sufficiently safe?", which deviates from standard considerations in the design of new bridges for engineers, may not be adequately addressed through conventional safety verification procedures provided by design codes such as Eurocode 3 [1]. Hence, this demands an alternative approach. Numerous nations have developed an approach for assessing the structural integrity of aged bridges. This novel technique employs partially calibrated safety coefficients, necessitating lesser requirements as compared to structures of new design. The process aims at providing a more accurate and reliable estimate of their resistance capabilities, as reported in studies [1–4]. The structural condition is comprehensively examined across four distinct stages, namely: preliminary investigation, in-depth studies, expert assessment, and remedial methodologies [5].

Each case requires a unique examination, grounded in on-site diagnostic tests. No two structural steels are alike; even minor variations in chemical composition or manufacturing parameters can lead to significant alterations in their properties. This is particularly true for structures built during the late 19^{th} and early 20^{th} centuries, a time marked by a lack of standardization and rapid advancements in metallurgical techniques. In fact, the period between 1892 and 1904 represents a transitional era from wrought iron to mild steel, with both materials often used in construction. The unique composition and history of these materials add further complexity to their evaluation [5].

Economic considerations also play an essential role in addressing these challenges. As these bridges have often withstood over 100 years of diverse environmental conditions, they represent the robustness of early steel constructions. However, the decision to preserve, maintain, or

renovate these structures must balance this historical value with practical and financial realities. Renovation is not always practical or financially feasible and can sometimes lead to only temporary extensions of a bridge's design life. In fact, in many cases, the cost of renovation can even exceed that of constructing a new bridge. Therefore, engineers need to understand and consider the immediate costs of investments alongside future maintenance and conservation expenses. This underscores the importance of considering economic factors in addition to structural integrity when assessing the future of these historic structures [2].

1.2 Study objectives

This research objective is to investigate the material composition and mechanical properties of a steel bridge built in 1908 in Norway. The goal is to compare these properties with modern steel standards and correlate them with results from existing literature to further identify and verify their characteristics. This approach aids in evaluating the feasibility of extending the operational lifespan of such historic structures.

Preserving these structures, instead of resorting to demolition, could present practical, environmentally friendly, and economically sound solutions. This approach, however, necessitates an understanding of these structures' remaining service life and their capacity to accommodate modern traffic loads. This task is particularly important for bridges constructed between the 1870s and 1940s, where material specifications often remain undocumented.

As an exploratory study, this thesis aims to enrich the current understanding of century-old railway bridges in Norway by providing comprehensive data on the iron or steel used in their construction. The research is envisioned as a pilot project that lays the groundwork for the analysis of other similar bridges from the early 20th century. The findings could not only form a basis for the development of precise evaluation techniques, but could also impact strategic decision-making regarding the safe, economical, and environmentally responsible preservation of these historic structures.

1.3 Bridge built in 1908

In collaboration with Bane NOR, this thesis focuses on an investigation of a 115-year-old riveted railway bridge, showing clear signs of wear and tear. The steel structure, originally located near Jevnaker, Norway, was delivered from the melting plant in 1908, as depicted in Figure 1. Having a short span of a little less than 4m

The bridge was originally constructed with a 'fixed track' system, which meant that the sleepers with rails were fixed directly to the beams, without any supporting layer of ballast or crushed stone. This structure inevitably led to pressure spots at the transitions of the bridge due to compression and crushing, resulting in impacts with passing trains and wagons that damaged the structure and its foundation. Over time, these issues necessitated frequent maintenance to maintain a smooth transition, making the design less efficient. In light of these challenges and the bridge's age, the ideal solution considered was to install a ballast system or replace the bridge with a pipe and ballast cover. Such a design could distribute stress more evenly and minimize maintenance. However, modifications had potential trade-offs. They might reduce the headroom and the opening area, which were critical considerations during the redesigning process. Moreover, if the new setup were to serve as a waterway, it would be essential to ensure that the pipes had sufficient capacity. Similarly, for animal passages, appropriate size adjustments would be required. Despite the rising interest in transitioning away from bridges with fixed tracks, a significant number of similar bridges are expected to remain operational in the coming years.

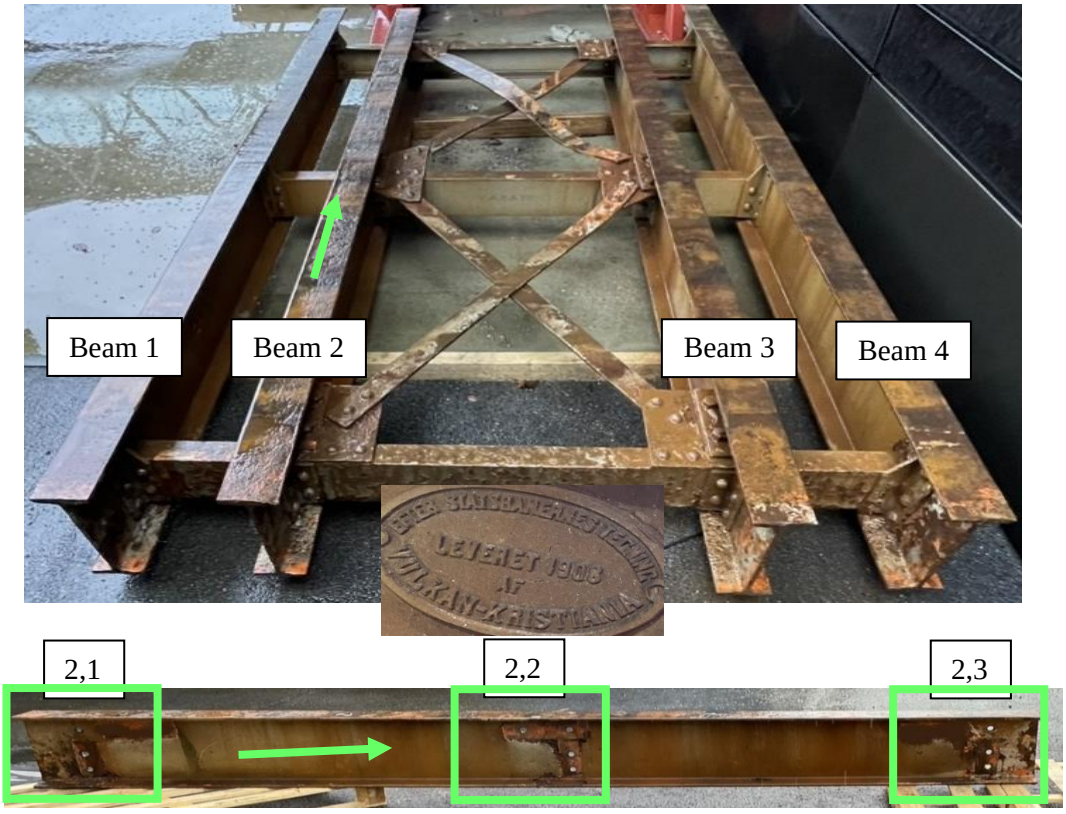

Figure 1: Bridge structure highlighting the sample extraction sites for material testing. The notation '2,1' indicates a sample from Beam 2, at location 1 along its span.

2. Literature review: materials in old metal bridges

2.1 Overview of materials used.

Bridges made of iron have been constructed since the industrialization era, which emerged in the late 19th century. Consequently, when dealing with older metal bridges, it is common to encounter structures that are over 100 years old. Remarkably, there are several bridges that have withstood the test of time since the 1850s, boasting an impressive lifespan of over 150 years. One examples of such a bridge is located in southern regions of Germany, namely the line between Waldshut and Koblenz, built in 1863 out of puddle iron [3].

Early metal bridges of the 19th century were primarily constructed from either cast iron or puddle iron, known as wrought iron. The production of puddle iron began at the onset of the 19th century. Its advantage over cast iron lay in its lower carbon content, which gave it a greater ductility. Such an increase in ductility provides an additional layer of safety as it makes the material less likely to fracture suddenly. This characteristic made puddle iron more suitable for forging processes and generally easier to work with. However, as the 19th century ended, puddle iron was surpassed by mild steel, which offered superior attributes in terms of chemical composition, cleanliness, and material properties. Mild steel exhibited enhanced qualities such as improved weldability and strength. By the turn of the 20th century, the primary material used in the construction of metal bridges was predominantly mild steel [2, 3].

During the rapid advancement of steel production and construction technology, including the bolting and welding of joints, there was a notable absence of testing methods to assess critical properties such as toughness, fatigue, and corrosion. These testing methods were not developed until much later in the 20th century, primarily focusing on modern steels rather than the older materials used in existing structures. As a result, our understanding of iron materials from earlier times remains fragmented, making the handling and evaluation of old metal structures more complex, which in turn is essential for the integrity assessment and determination of the remaining life of a given bridge [1, 3]. This is especially true for metal bridges built between 1870 and 1940.

Before the 1910s, the steel industry was characterized by a lack of standardization. Each steel manufacturer adhered to their own unique set of practices and formulas. Consequently, this led to a significant heterogeneity in the metals produced, particularly in terms of their chemical and mechanical attributes [2, 3]. An example of an attempt to establish some standardization can be found in the German railway authorities' regulations set in 1899 [6], which stipulated the specific materials to be used in the construction of iron railway bridges: mild steel was required for all structural components exposed to compression, tension, and bending, including rivets. On the other hand, cast iron was deemed appropriate only for minor elements exclusively, specifically those subjected only to compression and not requiring any form of workmanship [6].

The forthcoming sections present a literature review of the historical metal materials, specifically puddle iron and mild steel. These materials hold significant relevance for the 1908-produced beam discussed in this thesis.

2.2 Puddle iron and mild steel

Puddle Iron

Puddle iron, as previously mentioned, served as the first structural steel until mild steel replaced it at the end of the 19th century. The characteristics of puddle iron include low carbon concentrations and an abundance of undesirable elements like phosphorus and nitrogen, which contribute to its brittleness and accelerated aging [3].

The material was produced through a process known as 'puddling,' pioneered by Henry Cort in 1784, which involved decarburizing cast iron using slags. This refining process comprised two steps: puddling and forging. During puddling, elements like silicon, manganese, sulfur, and phosphorus were reduced in concentration through oxidation. The refined iron was divided into sections, known as blooms, hammered to remove any remaining slags, then fused together and shaped depending on the requirements [7]. Notably, the manufacturing process left mineral impurities, primarily silica slag, within the puddle iron [8]. These were embedded during the forging and stirring processes and were insufficiently removed. During rolling, these impurities aligned with the longitudinal direction, leading to inferior mechanical properties in the through-thickness direction of the products and giving the material a distinctive anisotropic nature. As a result, the puddle iron displayed significant microstructural heterogeneity, including a wide range of grain sizes and the presence of slag, sulfides, and oxides [3, 7].

Despite its inferior mechanical properties, puddle iron demonstrates commendable corrosion resistance, contributing to the longevity of structures built from this material. An appreciable variability can be expected in the material properties of puddle iron [3].

Mild Steel

Many old metal bridges that can be seen today are composed mainly of mild steels, also known as rimmed steel. These steels have undergone significant enhancements, particularly in strength properties, making them comparable to modern standards such as S235. However, when it comes to factors like toughness and weldability, one must proceed with caution due to consistently high concentrations of sulphur, phosphorus, and carbon revealed in their chemical composition [1]. Notably, mild steel displays a homogeneous grain structure [2].

The development of mild steel manufacturing processes effectively replaced the production of puddle iron, with specific type of process employed significantly impacting the material properties [3]:

- **Bessemer-Steel (since 1860):** The Bessemer process uses an air converter for refining, which introduces a high nitrogen content, making the steel susceptible to aging. In this process, air is blown through molten pig iron, oxidizing excess carbon and impurities such as silicon and manganese [2]. Notably, the resulting phosphorus content is higher compared to that in modern steels [3].

- **Thomas Steel (since 1880):** Thomas steel, similar to Bessemer steel, also contains high nitrogen content due to air converter refining. However, it is distinguished by lower phosphorus and sulfur contents. The Thomas process is essentially identical to the Bessemer process but is designed for high-phosphorus pig iron. This is made possible by using a basic lining based on dolomite (Thomas converter), producing basic Thomas steel [3].
- **Siemens-Martin Steel (since 1864):** Siemens-Martin steel is relatively pure with minimal contamination, lower nitrogen levels, but typically higher sulfur content, where excess carbon and impurities are burned out [2, 3]. A key advantage of mild steel is its significantly reduced non-metallic inclusions and material anisotropy compared to puddle iron, leading to greatly enhanced ductility and toughness values with less variability [2].
- **Chill mold casting**, a technique utilized in the late 19th and early 20th centuries, involved pouring molten steel into a chill mold to cool before rolling. This method produced steel with varying qualities due to distinct cooling rates and impurity distribution. The outer sections of the casting often consisted of nearly pure steel, while the center contained a higher concentration of unwanted alloys and impurities, as well as potential blister formations. Despite efforts to remove surface impurities before rolling, central impurities often remained undisturbed, resulting in inconsistent material properties across the steel component's cross-section. Consequently, steel produced using this method generally did not match the quality of today's construction steels due to these inconsistent material properties and a tendency for brittleness in the steel's core sections [1].

2.3 Characterizing metal railway bridge materials

The preservation of as many bridges as possible necessitates an understanding of their remaining lifespan, particularly where it is required to adapt design loads to accommodate for modern traffic. This task is critical for bridges built between the 1870s and 1940s, where material specifications often remain undocumented. Understanding the material properties of these aged structures is crucial for evaluating their structural integrity and predicting their remaining service life. To facilitate this, it is necessary to compile a database containing detailed information about the iron and steel used in these structures. Precise and effective evaluation techniques, demanding an accurate representation of the materials involved, are particularly required for these older bridges [1, 4].

Understanding a bridge's resistance to design loads and environmental influences throughout its lifespan requires a broad understanding of material properties. While strength and toughness parameters are of utmost importance, other characteristics like workability (e.g., weldability), hardness and resistance to corrosive effects also contribute to the durability and potential strengthening of the structure. However, it is important to note that fatigue properties, while typically essential for a comprehensive characterization, are beyond the scope of this study. Consequently, this thesis will focus on the following key parameters to typify the metal composition of a bridge [4]:

- Chemical composition
- Mechanical strength properties
- Toughness characteristics
- Fracture mechanics properties
- Hardness properties

2.3.1 Chemical profiling

In its raw form, wrought iron is not ideal for use as a construction material due to its high ductility and relatively low strength. However, the strategic introduction of minor quantities of certain elements can dramatically alter the steel's mechanical properties. It is remarkable how sensitively iron’s characteristics, in terms of both strength and ductility, react to alloy additives, a responsiveness not mirrored in other materials. Importantly, impurities and non-metallic inclusions in the alloy can significantly influence the properties of the resulting steel. These inclusions can be composed of slag or air and other gas-filled pores [3].

There is a need to distinguish between elements that enhance the steel's characteristics and those that negatively affect the final product. A detailed examination of the impact of various chemical elements on the steel's characteristics is displayed in Table 1 [3].

Chemical analysis of the steel offers valuable insights into both the production process and its subsequent weldability. For instance, the nitrogen content can provide insights into the likelihood of aging-induced embrittlement. Moreover, chemical analysis, when combined with Charpy toughness measurements such as 27J, chemical analysis can assist in categorizing steel into specific grades according to industry standards. Hence, the chemical assessment of steel plays a pivotal role [3].

Table 1: The impact of various chemical elements on material characteristics [3]

	C	Si	Mn	P	S	Cr	Ni	Mo	Al	N
Ultimate strength	+	+	+	+	-	+	+	+	+	+
Elastic limit	+	+	+	+	N/A	+	+	+		
Ultimate elongation	-	-	-	-	N/A	+	-	-	-	-
Hardness	+	+	+	+	N/A	+	+	+	+	N/A
Hardenability	+	+	+	N/A	N/A	+	+	+	N/A	N/A
Toughness (Charpy V impact energy)	-	-	+	-	-	-	+	-	N/A	-
Arc weldability	-	-	+	-	-	-	N/A	+	-	-
Thermal resistance	+	+	N/A	+	-	+	+	+	N/A	N/A
Corrosion resistance		+	N/A	+	-	+	+	+	N/A	N/A
+ increase in material characteristics **- decrease in material property** **N/A: no data available**										

Weldability

The variability of old structural irons and steels can largely be attributed to the empirically driven manufacturing processes, resulting in greatly varied chemical and mechanical properties. This inhomogeneity extends to the cross-section of a member, as it could contain substantial impurities and segregations within the plates or profiles. One particularly concerning consequence is the potential concentration of impurities in the heat-affected zone during thermal processes such as welding or flame cutting, which can result in damage like cracks [1]

While welding can often simplify the repair and strengthening of old steel structures, its applicability varies across different steel types due to the lack of standardization in early 20th-century steel production, as previously mentioned. Certain types, like wrought (puddle) iron and early mild steels, present significant challenges for welding due to factors such as substantial slag inclusions and high nitrogen contents, respectfully [1]. Early steels possess certain inherent characteristics that render them unsuitable for welding applications. One such attribute is the material's inconsistent toughness, which can lead to the formation of cracks. These cracks are often the result of residual stresses originating from the weld's heat-affected zone.

Given the inherent heterogeneity in old steels, even for seemingly identical cross-section, it's difficult to predict the properties of one part of a structure from another, underscoring the need for comprehensive weldability testing before initiating repair or strengthening tasks. This process involves an initial assessment based on any existing welds, followed by comprehensive tests on samples for factors such as ductility and chemical content [1].

Furthermore, the weldability of the material can be evaluated by examining its chemical composition, paying special attention to the contents of carbon, phosphorous, and sulphur, as these elements can notably affect the steel's weldability. Additionally, metrics such as the carbon equivalent (CEV) can offer insights into weldability, but in some instances, these may not be adequately informative, necessitating the use of more accurate evaluations such as cold-cracking tests. Example of such destructive tests are Tekken and controlled thermal safety (CTS) test. In conclusion, any attempt to work with early steels should begin with a thorough understanding of their properties to ensure the feasibility of the desired operations [1].

Iron-Carbon Equilibrium diagram

Steel, primarily made up of iron and carbon, uses various alloying elements to enhance its mechanical properties. The interaction between iron and up to 2% carbon in carbon steel generates distinct phases, including ferrite, a soft and ductile phase, and cementite, a hard and robust phase. Other complex phases like pearlite, martensite, and bainite can also form under different conditions of temperature and carbon concentration [9].

The iron-carbon (Fe-C) phase diagram is an essential reference for comprehending the performance characteristics of carbon steel. This diagram forms the foundation for relating heat treatment processes, microstructural variations, and mechanical properties in iron-carbon alloy systems. Figure 2 a) illustrates a section of the phase diagram for carbon compositions less than 2% and temperatures below 1000°C, the range that defines wrought steels, which are critical for most engineering applications. Figure 2 b) showcases the iron-rich side of the Fe-C diagram (most relevant part for this study), illustrating the wide reach of the ferrite phase region and the decline in carbon solubility as temperature decreases [9].

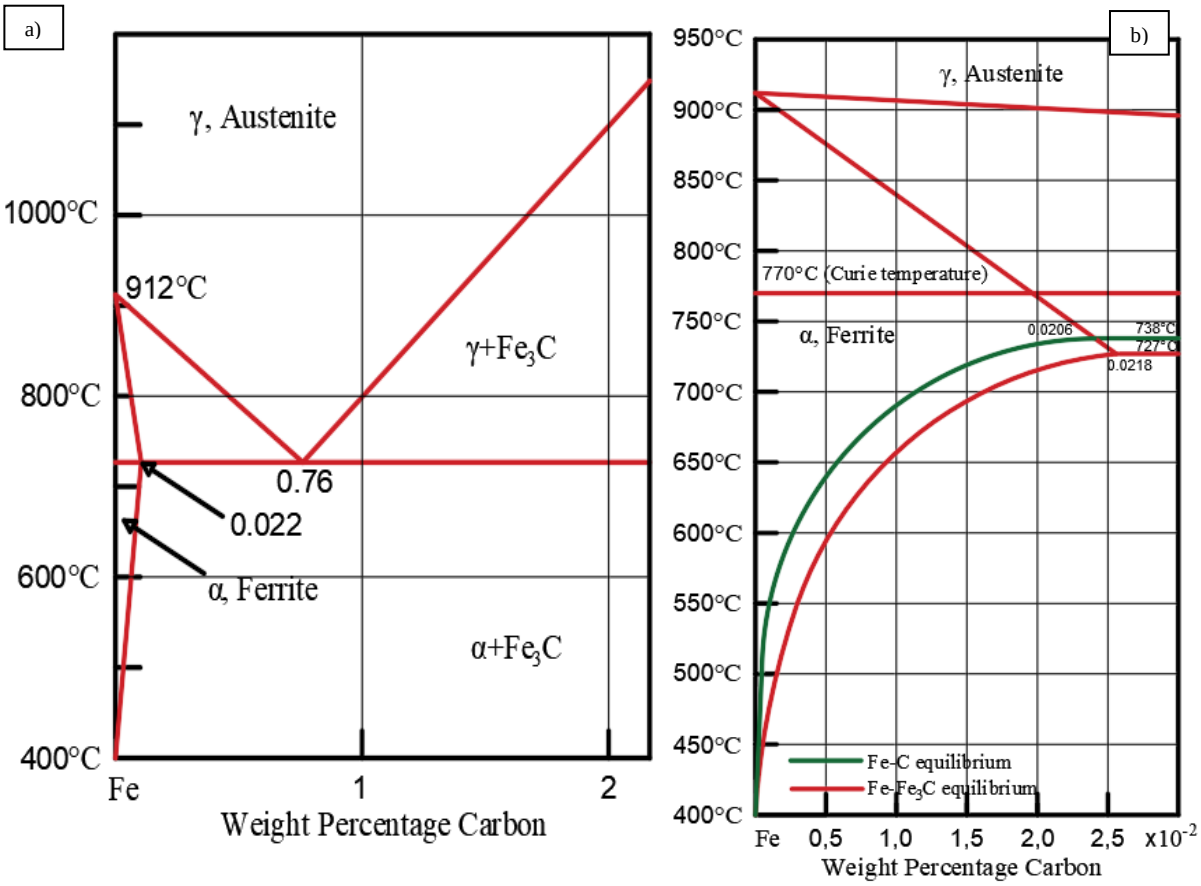

Figure 2: in a) and the iron-rich side of the Fe-C diagram is illustrated in b) [10]

At ambient temperatures, the stable phases of steel comprise of ferrite and pearlite, where pearlite is a lamellar structure consisting of alternating layers of ferrite and cementite. Ferrite,

a common constituent in steels, has a less densely packed body-centered cubic (bcc) structure. Cementite, on the other hand, is an exceptionally hard and brittle compound that enhances the strength of steels. All steel alloys, up to 2% carbon content, transition through the austenite phase during cooling. Austenite is a high-temperature phase with a densely packed face-centered cubic (fcc) structure. The process of heating carbon steel into the austenite region is termed austenitization. The austenitization temperature drops with increasing carbon content up to the eutectic concentration of 0.76% C, after which it rises for higher carbon content up to 2% C. Austenite is nonmagnetic and can be sustained at room temperature by incorporating suitable alloying elements like manganese and nickel. Various thermal treatments results in different room-temperature microstructures. For example, gradual cooling is likely to produce a softer ferrite microstructure [9].

Ferrite contains a minimal quantity of carbon, with the maximal carbon solubility in iron being 0.022% at 725 °C. The iron-carbon phase diagram illustrates the transformations that occur when a specific grade of carbon steel undergoes slow heating or cooling. For instance, eutectoid steel converts entirely to austenite upon heating above the eutectoid temperature of 725 °C and transforms completely into pearlite when cooled below this threshold [9].

Carbon content introduces a multitude of steel compositions and microstructures, is a key factor in determining possible steel properties. Notably, strength increases with carbon content up to the eutectoid composition, but then begins to decline as a brittle cementite forms a grain-boundary network [9].

The majority of carbon in steel is represented as iron carbide within the microstructure. Therefore, the broad range of properties in non-heat-treated steel is largely dictated by the relative quantities of iron and iron carbide in the microstructure. Increasing the fraction of iron carbide in steel, while keeping the microstructural attributes constant, results in harder and stronger steel. While carbon is the principal element that metamorphoses iron into steel, other elements are also added to create a variety of favorable properties. These alloying elements influence the iron-carbon phase diagram by shifting its phase boundaries and modifying the forms of the phase areas. The eutectoid reaction, which happens at 725 °C for unalloyed steel, is significantly impacted by the type and concentration of the alloying elements [9].

2.3.2 Assessing mechanical strength

The mechanical properties of structural steel, including yield strength, ultimate strength, and elongation, serve as critical indicators of its strength. These characteristics are usually determined from a tensile test on standard specimens. Figure 3 a) illustrates a behavior featuring a unique yield plateau, referred to as the yield limit, and can be measured in two distinct ways depending on the standard applied. In older standards, emphasis was placed on measuring the lower yield limit of the steel, denoted as R_{eL}, whereas modern standards typically use the upper yield limit, represented as R_{eh} or f_y, to indicate the steel's yielding capacity.

Following the yield phase, the steel undergoes plastic deformation and hardening until it reaches its ultimate strength, denoted as R_m (f_u) in the figure, which corresponds to the peak value on the stress-strain curve.

In Figure 3 b) it can be seen that the stress strain curve does not exhibit a distinct yield plateau. In such cases, an elongation of 0.2% is used to define an equivalent yield strength, termed as $R_{p0,2.}$ The ultimate strength, is similar to that in the initial figure. This type of stress-strain behavior, lacking a clear elastic limit is often the case with older steels and cold-rolled or cold formed materials.

Tensile tests are performed by exerting a pull force on a steel plate or rod at a controlled rate. The procedure for conducting a tensile test is elaborated in ISO 6892-1:2019 standard [10].

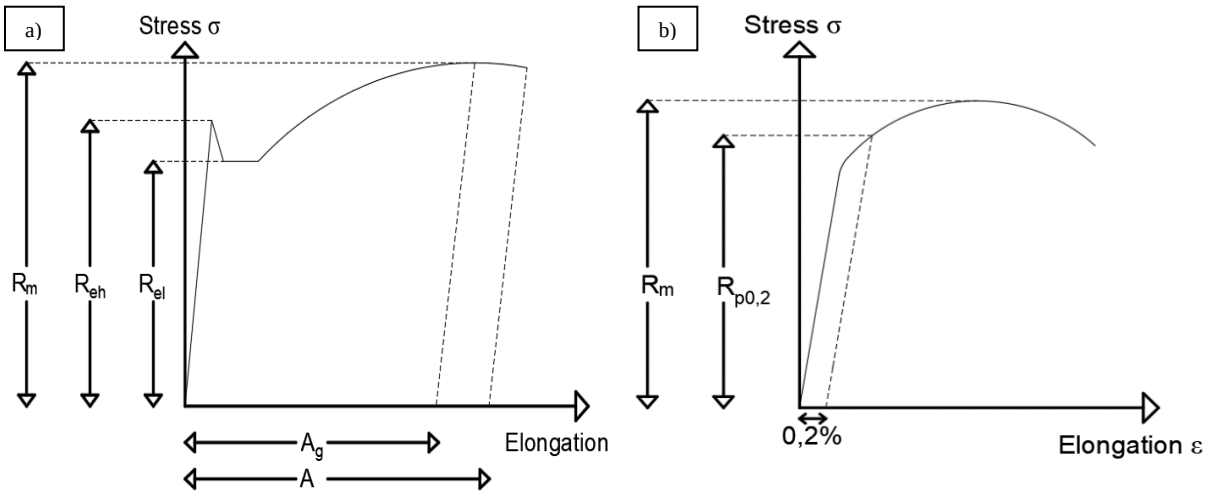

Figure 3: Stress-strain graph showcasing distinct (a)) and indistinct elastic limits (b))

Parameters given are as follows:

- R_{eL}: lower elastic limit (old standard for yield strength f_y) [MPa]
- R_{eH}: higher elastic limit (current standard for yield strength f_y) [MPa]
- $R_{p0,2}$: yield strength at 0.2% elongation [MPa]
- R_m: ultimate tensile strength (f_u) [MPa]
- A_g: elongation before reduction of area of the specimen [mm]
- A: elongation at failure [mm]
- E: elastic modulus (f_y/ε) [GPa]

2.3.3 Material toughness

Charpy impact tests are typically used to determine the material's ductile-to-brittle transition temperature (DBTT), the temperature at which a material switches from ductile to brittle behavior. One of the simplest methodologies for estimating fracture resistance is a notch toughness experiment [11]. To some extent, Charpy test values can provide insight into a material's fracture toughness. However, the guidelines provided by BS 7910 for these calculations may not be ideal. A key reason for this is that the Charpy specimen does not have a sharp crack. Instead, it features a V-shaped notch that introduces stress concentrations at its tip.

Transitional fracture behavior is typically characterized by two key criteria: the quantity of energy absorbed to fracture a specimen (a minimum of 27 J for V-notch specimens), changes in fracture appearance, shifting from fibrous (plastic) to brittle (at least 50% cleavage fracture). When documenting the transition temperature, it's crucial to include the determining criterion (T_{27J}, $T_{50\%}$) [11].

Per the Eurocode EN 1993-1-10 [12] and product standards such as EN 10025-2 [13], the minimal impact energy at a given temperature, denoted as T_{27J}, should not fall below 27 J for Charpy V specimens, regardless of the subgrade. These code stipulations are advisable when selecting steel for new structures, but do not refer to structures already in operation. A temperature curve (K/T curve) shows the energy absorbed as a function of the test temperature for a particular test piece in Figure 4. This figure can be split into three distinct regions:

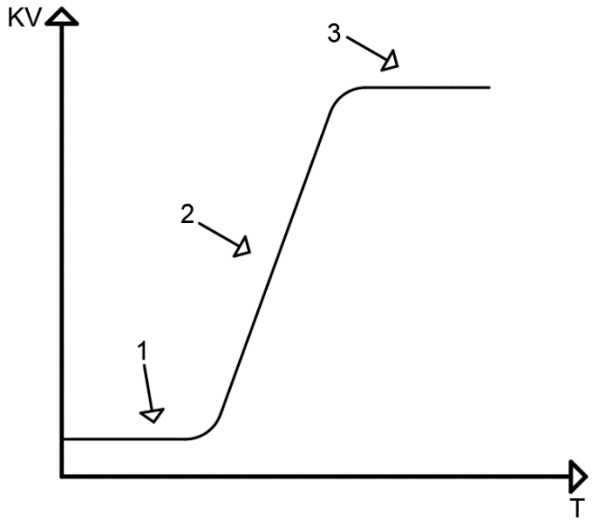

Figure 4: Absorbed energy/temperature curve shown schematically

(1) Upper-shelf zone, exhibiting ductile behavior
(2) Transition zone
(3) Lower-shelf zone, showing brittle behavior

Toughness values are considered essential indicators of steel's mechanical properties. The transition temperature is practically significant as it indicates the material's performance under impact loading and signifies the temperature at which abrupt brittle fracture might occur, especially in the context of older bridge structures. Steel, for instance, may behave quite ductile at one specific temperature, but become brittle as the temperature decreases. This dual behavior emphasizes the importance of Charpy tests in evaluating these materials' properties under varying environmental conditions. It reflects the effects of material aging, which can increase the tendency for brittle fracture, elevate the transition temperature, and harden the material, leading to a reduction in plastic deformation capacity. This temperature also rises under the influence of fatigue, pulsating actions, and dynamic actions, factors frequently encountered in bridge operations. Moreover, operations often occur at lower temperatures for extended periods, impacting the transition temperature. The presence of numerous stress concentrators in the form of non-metallic inclusions in mild steels, coupled with changes due to microstructural degradation processes, also comes into play. In light of these considerations, a comprehensive understanding of material factors enables a more precise evaluation of durability in long-serving bridge structures [11].

2.3.4 Hardness

In engineering terms, hardness is primarily characterized as a material's resistance to indentation. Indentation, achieved by pressing a hard point or ball onto a material with a specific force This action results in a depression due to plastic deformation. Different aspects of the indentation, such as its depth or size, are then used to measure the hardness of the material [14].

The Vickers hardness test, chosen for the thesis, employs a diamond-tipped pyramid-shaped indenter. This pyramid has a square base with a face angle of $\alpha = 136°$. This specific design ensures that the penetration depth equates to roughly one-seventh of the diagonal length of the indentation. To calculate the Vickers hardness number (HV), the applied force (P) is divided by the surface area of the indentation, as per the equation:

$$HV = \frac{2P}{d^2} sin\frac{\alpha}{2}$$

Importantly, due to the standard pyramid shape of the indenter, the test is expected to provide a hardness value that does not depend on the size of the applied force. As a result, a broad range of forces, usually between 0.1 and 120 kg, can be used. This range allows the hardness of nearly all solid materials to be measured on a single scale [14].

2.3.5 Existing studies on old steel properties

The data collected for this section comes from the research of Cremona et al. and the "Sustainable Bridges" project, with all findings presented in Tables 2-7 [3]. These studies provide valuable insights into the properties of steels used in various German bridges from the late 19th century to the mid-20th century.

This information serves as a reference point for analyzing and comparing the material used in this current study, which focuses on an unidentified steel from a similar historical period. An understanding of these previous studies can help shed light on potential similarities and differences in the properties and behaviors of the steel used in old Norwegian structures.

Table 2 to 5 presents the chemical composition of both puddle iron and mild steel, studied in the above-mentioned reports. The entries in the table provide a snapshot of the typical elements and their respective proportions found in steels of the era. Knowledge of the chemical composition is crucial, as it directly impacts the steel's physical and mechanical properties.

Tables 6 (puddle iron) and 7 (mild steel) focus on the mechanical properties of the old steels. These tables provide data on critical parameters such as yield strength, tensile strength, and elongation, among others. The listed mechanical properties, tested under standardized conditions, give an indication of the performance characteristics of these steels.

Table 2: Mean concentrations [%] of chemical elements in puddle iron (wrought iron) [3]

Reference	C	Si	Mn	P	S	Cr	N	Cu	Ni	Al
[15]	0.043	0.074	0.207	0.183	0.051	0.028	0.009	0.056	n.s.	0.001
[16]	0.048	0.077	0.061	0.325	0.031	n.s.	n.s.	0.042	0.046	n.s.
[17]	0.018	0.1	< 0.1	0.47	0.056	n.s.	0.007	n.s.	n.s.	n.s.
[2]	<0.08	n.s.	<0.4	<0.6	<0.04	n.s.	n.s.	n.s.	n.s.	n.s.

n.s.: not specified

Table 3: Mean concentrations [%] of chemical elements in mild steel [3]

Reference	C	Si	Mn	P	S	Cr	N	Cu	Al
[15]	0.162	0.017	0.599	0.052	0.042	0.006	0.01	0.104	0.001
[16]	0.048	0.077	0.061	0.325	0.031	n.s.	n.s.	0.042	n.s.
Thomas [2]	0.02-0.1	>0.08	0.3-0.5	0.04-0.12	<0.1	n.s.	n.s.	n.s.	n.s.
S-M [2]	0.05-0.15	n.s.	0.2-0.5	0.03-0.06	0.02-0.15	n.s.	n.s.	n.s.	n.s.

S-M: Siemens Martin process

n.s.; not specified

Table 4: Mean concentrations [%] of chemical elements in puddle iron, various authors [18]

Reference	C	Si	Mn	P	S
[19]	0.021	0.09	0.06	0.37	0.021
[20]	0.07	0.1	n.s.	0.016	n.s.
	0.12	0.11	0.14	0.2	n.s.
[21]	0.10	0.06	0.01	0.25	0.03
	0.11	0.11	0.01	0.11	0.01
	0.02	0.15	0.03	0.12	0.02
[22]	0.001	0.056	0.013	0.28	0.037
	0.003	0.021	0.0092	0.092	0.006
	0.015	0.030	0.070	0.067	0.003
	0.024	0.035	0.095	0.286	0.010
	0.001	0.034	0.097	0.283	0.014
	0.001	0.110	0.146	0.287	0.010
	0.003	0.068	0.108	0.317	0.018
	0.170	0.021	0.487	0.012	0.056
	0.007	0.001	0.373	0.035	0.034

n.s.: not specified

Table 5: Mean concentrations [%] of chemical elements in mild steel, various authors [18]

Reference	C	Si	Mn	P	S	Process
[22]	0.1-0.12	0.08-0.1	0.25-0.3	0.06-0.08	0.05-0.06	Bessemer
	0.1-0.2	0.08-0.15	0.4-0.5	0.06-0.08	0.05-0.06	Bessemer
	0.13	0.01	0.47	0.066	0.037	Thomas
	0.05-0.1	<0.005	0.3-0.5	0.05-0.08	0.04-0.07	Thomas
	0.05-0.09	<0.005	0.3-0.4	0.05-0.08	0.04-0.07	S-M
	0.13	0.15	0.46	0.016	0.019	S-M
[23]	0.09	0.02	0.37	0.04	0.05	S-M
	0.62	0.14	0.89	0.04	0.05	S-M
[19]	0.038	0.01	0.4	0.65	0.044	1910(1)
	0.05	0.01	0.4	0.041	0.034	1936(1)
[24]	0.15	0.02	0.27	0.068	0.02	1900(1)
	0.04	0.01	0.4	0.047	0.037	1922(1)
	0.15	0.01	0.81	0.06	0.062	1940(1)

(1): No data available for the steel producing process, only year of production

S-M: Siemens Martin process

Table 6: Tensile tests on old steel bridges made of puddle iron (wrought iron) from [15]

Parameter	Yield strength [MPa]	Tensile strength [MPa]	Elongation [%]
Mean value	283.6	389.1	24.86
Standard deviation	40.6	36.5	8.46
Number of samples	99	99	90

Table 7: Tensile tests on old steel bridges made of mild steel collected from [18]

Parameter	Process	Yield strength [MPa]	Tensile strength [MPa]	Elongation [%]
Mean	S-M	282	417	27
	Thomas	282	409	27
	N/A	272	417	25
Standard deviation	S-M	19.6	13.8	3.1
	Thomas	12.8	10.3	1.5
	N/A	28.9	28.9	3.1
Number of samples	S-M	481	487	485
	Thomas	680	680	680
	N/A	90	90	90

S-M: Siemens Martin process

N/A: No data available for the steel producing process, assumed to be general old mild steel

2.4 Current codes for Norwegian steel structures

The details related to material properties and the associated partial coefficients, as provided in Norwegian codes, are largely targeted towards road bridges, considering that its publisher is the Norwegian Road Administration. This information can be found in the handbook named: "V413, Bæreevneklassifisering av bruer, materialer" [25], where control of capacity is carried out in accordance with NS-EN 1993 [12], with subsequent material factors (see Table 8) and material strengths (see Table 9).

Over time, permissible stresses have varied quite a bit. As an example, it can be mentioned that steel with quality St. 37 in 1910 was utilized to approx. 800 kg/cm2, in 1920 to 1000 kg/cm2, in 1930 to 1200 kg/cm2 and in 1954 to 1350 kg/cm2. This is because the quality of the steel has improved over the years, while knowledge about the use of steel as a construction material has increased [25].

If documentation from steel certificates is accessible, it may be utilized, but exclusively for the material' lowest strength. It is then necessary to evaluate whether the steel certificates are applicable to all structural components. In the absence of such a certificate, the subsequent guidelines should be used as a basis [25].

Table 8: Tensile strength and yield strength for construction steel [25]

Age	Steel quality	Tensile strength	Yield strength
		f_u [N/mm^2]	f_y [N/mm^2]
Pre 1920	All steel	350	220
After 1920	St. 37 (S235)	370	235
	St. 42	420	255
	St. 44	440	265
	St. 52	520	345

For bridges constructed prior to 1920 where the steel quality remains unknown, it is assumed to be of the St. 37 standard. An exception to this assumption arises for bridges constructed in accordance with the regulatory class SVV 1958, where either St. 42 or St. 52 steel quality can be selected based on the diagrams provided in Appendix A (in handbook V413), given that the span, quantity of beams, and beam dimensions are known [25].

Table 9: Material factors for steel structure in ultimate limit state [25]

Material	Material factor	
	γ_{M0}/γ_{M1}	γ_{M2}/γ_{M3}
Construction steel		
Pre 1920	1.50	1.70
	1.35	1.50
	1.35	1.50
After 1920	1.20	1.35
After 1920 with material certificate, lowest f_y	1.15	1.30

2.5 Understanding buckling behavior

2.5.1 Members in compression

Compression members, like tension members, are structural elements that respond to axial loads. Their performance under axial compression relies on their cross-sectional resistance and susceptibility to instability. Generally, these steel members are of medium to high slenderness, making instability a key design consideration. The modes of failure for these members include yielding of the cross-section, local buckling of thin-plate compression elements, and overall flexural buckling.

Very robust compression members typically fail when yielding of the cross-section occurs, behaving elastically until reaching a plastic state at the crushing load, i.e., the maximum compressive load based on their cross-sectional area and material yield strength. However, the member's resistance can be reduced due to local buckling of thin-plate elements, depending on the plate's length-to-thickness ratio and yield strength.

Nevertheless, the resistance of compression members is generally determined by their slenderness. An increase in slenderness significantly reduces their capacity, leading to potential failure due to overall flexural buckling. The decline in resistance stems from the applied compressive load N, causing lateral bending in a member with initial curvature.

For a perfectly straight elastic member, no bending occurs until the critical elastic buckling load (N_{cr}) is reached, at which point lateral deflections increase until failure, known as flexural buckling. Therefore, the critical elastic buckling load serves as a measure of the member's slenderness, while the crush load provides an indication of its resistance to yielding.

2.5.2 Beams under stress

Beams functions as critical structural elements, engineered to withstand bending moments and shear forces throughout its span by transferring the transverse loads they carry to the supports of its structure. Applied forces could lead to various failure modes such as: yielding and or fracturing of flange depending on if in compression or tension, shear yielding, bearing failure, local buckling and global buckling. Where the beam's performance heavily relies on cross-sectional capacity, its yield strength and susceptibility to lateral-torsional buckling. The beam's ultimate strength is reached when the cross-section experiencing the maximum moment yields fully, forming a plastic hinge. This moment capacity M_p is higher than the yield moment M_y. Alternatively, in deep, short-span beams where shear forces dominate, the strength is determined by the shear force causing the web to reach a fully plastic state [26].

The initial evaluation in figure above assumed that a beam primarily deflects within its stiffer principal plane under stress, vertically. However, in the absence of sufficient lateral support or inherent lateral stiffness, the beam may divert from this behavior, resulting in out-of-plane buckling. Notably, the magnitude of the force causing this buckling could be much less than what the beam can resist within its load-bearing plane [26]. This behavior is also known as lateral-torsional buckling, an instability mode especially prone to members with open and slender section such as I or H sections about their major axis, where their respective compressed flange deforms laterally, characterized by the elastic buckling moment M_{cr} [27].

3. Experimental procedures

3.1 Preparing test samples

To conduct an analysis of the 115-year-old material with its unknown properties, it was vital to carry out metallographic preparations. The initial step involved assessing the bridge section supplied by BaneNor to determine the optimal method for disassembly and sample extraction. To minimize any unnecessary heating, consequently affecting the steels properties, a magnetic drill was employed to remove the rivets securing the structural members.

Beam 2, located at the center of the bridge section and having endured substantial stress during its service life, was selected for sample extraction. Given the substantial length of the I-beam and cross-sectional area, material scarcity was never a concern. The focus then shifted to identifying areas of interest for further study. The I-beam was cut into manageable lengths of approximately 0.5 meters, specifically targeting one end and the middle. Additional cutting was executed to separate the web from the flanges of the beam, designated as sample locations. To prevent any mechanical deformation, all cuts were setup at a low feed-rate, with abundant amounts of coolant assisting in the process. As anticipated, corrosion was observed on each specimen, particularly those situated at the bottom flange. This necessitated the use of sandblasting, which revealed localized corrosion as depicted in Figure 6 e).

Table 10: Summary of test samples, extraction locations, and orientations

Specimen location	Tensile	Charpy impact	Hardness	Microscopy	LTB
2,1T (Top flange at end of Beam 2)	3^{L}	9^{L}	2	2	-
2,1B (Bottom flange at end of Beam 2)	3^{L}	$9^{L}/0$	2	2	-
2,2T (Top flange at middle of Beam 2)	4^{L}	9^{L}	3	2	-
2,2W (Web at middle of Beam 2)	4^{L}, 4^{T}	9^{L}	3	2	-
2,2B (Bottom flange at middle of Beam 2)	4^{L}	9^{L}	3	2	-
Beam 1 (Full length)	-	-	-	-	1
Beam 3 (Full length)	-	-	-	-	1
Beam 4 (Full length)	-	-	-	-	1
Total amount of samples/tested	22	45/36	13	10	3

Note: ^{L} and ^{T} denote the sample orientation, specifically longitudinal (rolling direction) and transverse.

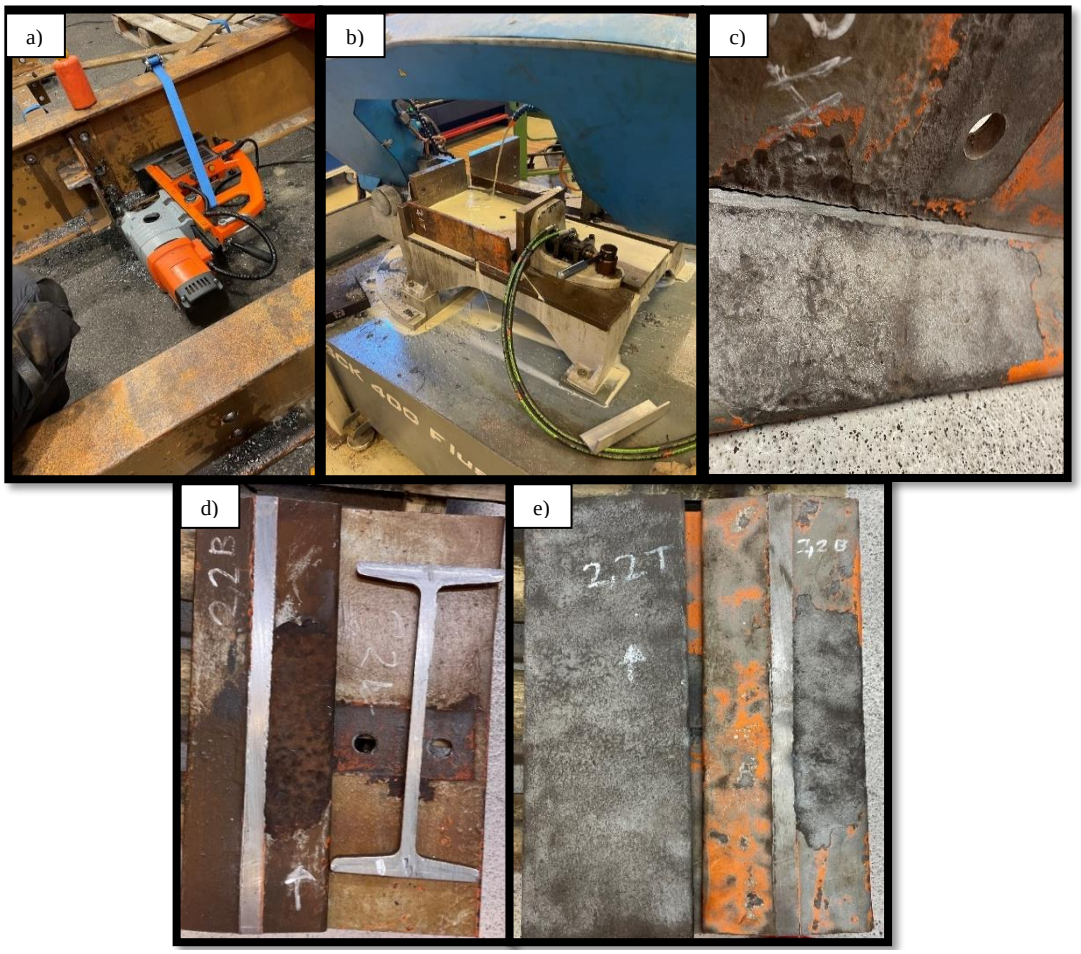

Figure 5: Procedure of dismantling and segmenting the beam for sample extraction

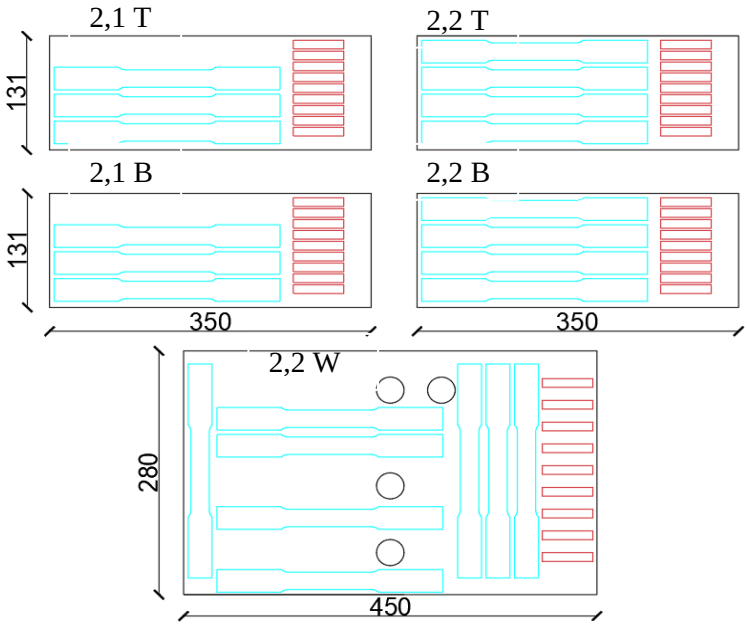

Figure 6: Model of samples created with the assistance of a CNC machine and Struers Discotom 100

3.2 Methods overview

3.2.1 Chemical composition and microstructure

A strip with a thickness of a few millimeters were cut along the width of its respective specimen and further cut into smaller pieces using Struers Discotom 100 at various locations in the cross section as shown in Figure 8. After the cutting, samples were carefully cleaned and rinsed with both water and ethanol to eliminate any potential contaminants. These specimens were then hot-mounted in multifast, a selected mount resin, using the Struers Citopress-30, resulting in a flat-surfaced cylinder, providing ease of handling, and mounting for grinding and polishing. The grinding and polishing stages were performed using a Struers Pedemax-2 machine while adhering to the guidelines outlined in the ASTM E03-11 standard [28].

Table 11: Complete procedure of the Struers method D

Step	Grinding and polishing	Lubricant	Time
1	Piano 220 µm	Water	2 min
2	Allegro	Allegro/Largo 9 µm	3 min
3	Dac	Dac 3 µm	3 min
4	OP-S	OP-S 0.25 µm	2 min

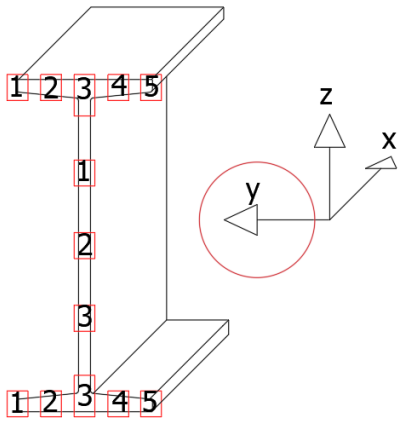

Figure 7: Orientation of extracted samples for microstructural and hardness analysis, as marked in the Y-Direction of the steel cross-section

As the final preparatory step, the metallographic samples were subjected to an etching process with Nital. This solution, a mixture of 6% nitric acid and ethanol, was applied for an approximate duration of 20±1 seconds, a timing determined to deem good results from experimental iterations. Post-etching, the samples were inspected under a light optical microscope (LOM) utilizing the bright field method. The integrated software Olympus Stream, in conjunction with quantitative metallography techniques, was utilized to determine the average grain size and phase content.

Weldability

Alongside these steps, an investigation into the steel components' weldability was carried out. This was done by assessing their resilience to hot and cold cracking, in line with the standard formulas proposed by the International Institute of Welding and corroborated by relevant academic literature [29-31]. A chemical composition examination facilitated the estimation of the metallurgical and structural weldability of the steel. Specific coefficients were identified based on the established methodologies outlined in the cited sources [29-31]. These coefficients are integral to the following discussion. Here is a simple explanation of the formulas applied for weldability calculations:

- The Carbon Equivalent (Ce) formulas predict the risk of hydrogen-induced cracking (HIC) in steel. A high Ce value suggests a higher risk of HIC [32]
- "Hot cracking" indicates cracks forming under high temperatures. The Hot Solidification Cracking (HSC) formula estimates the risk. A high HSC value denotes improved resistance to hot cracking, essential for the structural and material's endurance under high-temperature operations [32].
- Carbon equivalent for cold cracking (C_e') denotes an important value. Cold cracking, which typically happens around room temperature, is typically synonymous to hydrogen-induced damage and can happen in two ways: along the grain boundaries (intergranular) or across them (transgranular) [32].
- The Heat-Affected Zone (HAZ) is the non-melted metal region near a weld that has undergone changes in its properties due to exposure to welding heat. Monitoring the hardness of the HAZ, which can increase because of the heat cycles of welding, is a crucial aspect of the process [32].

Carbon equivalent value (C_e):

$$C_e = C + \frac{Mn}{6} + \frac{Cr + Mo + V}{5} + \frac{Ni + Cu}{15} < 0.41 \quad (1)$$

Hot cracking resistance (HSC):

$$HSC = 100\left(S + P\frac{Si}{25} + \frac{Ni}{100}\right) + \frac{C}{3Mn + Cr + Mo + V} < 4.0 \quad (2)$$

Carbon equivalent for cold cracking ($C_e´$):

$$C_e' = C + \frac{Mn}{6} + \frac{P}{2} + \frac{Mo}{4} + \frac{Ni}{15} + \frac{Cu}{13} + \frac{Cr + V}{5} + 0.0024t < 0.4 \quad (3)$$

Heat-affected zone (HAZ) hardness:

$$HV_{max}' = 1200C_e' - 200 < 300HV \quad (4)$$

Hardness range after welding:

$$HV_{max} = 90 + 1050C + 47Si + 75Mn + 30Ni + 31Cr < 350HV \quad (5)$$

3.2.2 Tensile strength testing

The tensile test specimens were precisely fabricated using CNC machining to meet the specifications stipulated in Annex D (thickness greater than 3mm) of the NS-EN ISO 6892-1:2019 standard [10]. Each test was performed at room temperature using the Zwick Roell tensile strength machine.

Prior to initiating the tests, the specimens were thoroughly examined for any potential cracks or inconsistencies, and measurements of thickness and gauge length were taken. The thickness of each specimen was assessed at a minimum of three points to ensure standard compliance. Following these preparatory steps, the testing machine was readied for operation.

The conditions for executing computer-controlled tensile testing adhere to the standards set by NS-EN ISO 6892–1. The testing speed was initially set at 0.015 mm/mm/min until a 0.2% yield strength was recorded. Subsequently, the machine speed increased to 0.1 mm/mm/min, maintaining this rate until fracture occurred. Upon fracture, the reduced area, along with the observed material behavior of each sample, was automatically calculated using the built-in "testXpert" software.

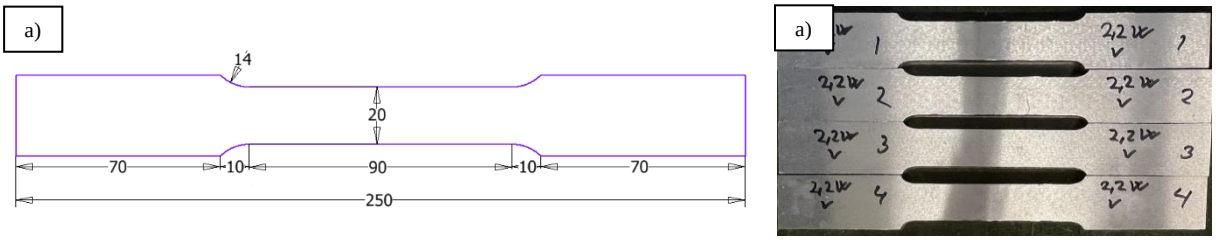

Figure 8: Tensile test sample drawing a) and finished batch from specimen 2,2 W b)

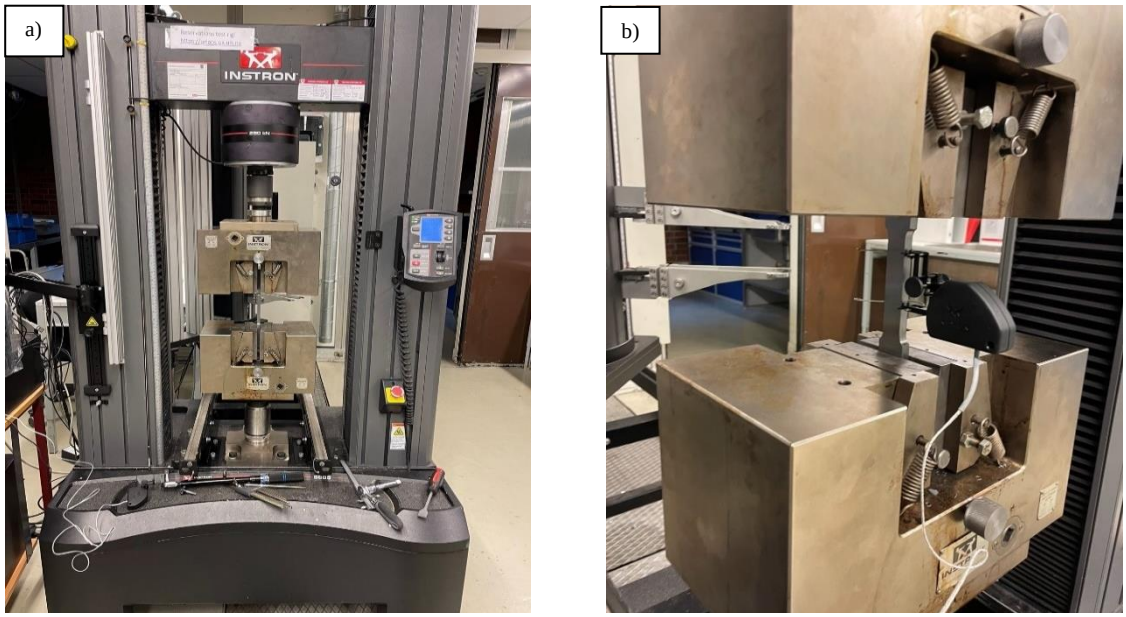

Figure 9: Instron tensile testing machine a) alongside a sample prepared for testing with the extensometer secured b)

3.2.3 Notched bar impact tests

Impact strength tests are carried out in accordance with the NS-EN ISO 148-1:2016 standard [33] at ranging temperatures (-20°C to +20°C). Each specimen was tested with nine V-notch samples, evenly distributed across the three temperatures. Out of a total of 45 test pieces, 36 underwent testing, each clearly labeled at both ends with a steel scribe.

The tests were carried out on standard samples, featuring a specific V-notch shape and dimensions with the standard as a guideline. Each sample had a square cross-section with 10x10mm dimensions.

Material sections were prepared into test samples using equipment designed to avoid local overheating or cold compression, as these could negatively affect the impact strength test results. Therefore, the Struers Discotom 100 was utilized, with its built-in function for interval cuts of 10.1mm in the material, followed by surface grinding and careful gauging to ensure compliance with specified tolerances. Nevertheless, all nine samples from 2,1 B failed to meet these standards and were thus discarded. Notches were formed through a cutting process, with all notch dimensions, such as depth, edge opening angle, and the radius of notch bottom rounding, carefully following the guidelines set out in the reference standard [33], due to their significant influence on the test outcomes.

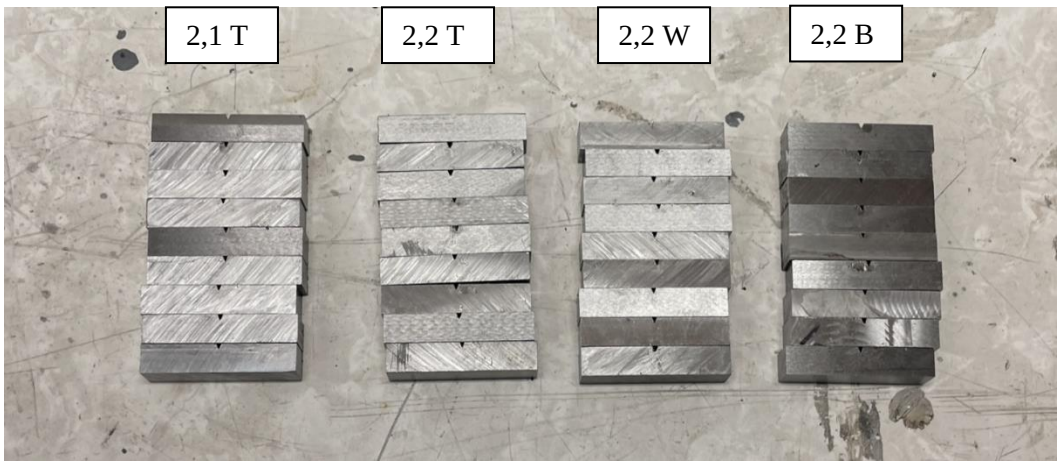

Figure 10: The selected set of samples deemed suitable for the impact test, meeting all required criteria for validity

3.2.4 Hardness testing

Utilizing the Innovatest Falcon 5000, hardness tests were conducted with a 10 kg HV force. The apparatus's integrated software enabled the gathering of sample overviews and aided the configuration of a grid for each respective one with the desired number of indentations. This was executed in compliance with the ISO-648 standard concerning the spacing and distance from the sample edge. Following the initial setup, the process transitioned to a fully automated stage, only requiring manual intervention to identify and rectify any anomalies in the measured hardness values.

In total, around 500 indentations were created with a dwell time of 10 seconds each. Initial tests comprised of 12 indentations per sample across various cross-sectional areas, assessing potential differences between the edge and middle of the flange and along the web. The results demonstrated a consistent distribution of hardness values throughout the flanges and the web. Three specimens (from the top flange, web, and bottom flange) underwent more comprehensive testing, with the maximum number of feasible indentations applied. Each 30mm diameter sample had between 80 and 110 indentations. However, due to a software error, data from one web sample with around 90 indentations was lost. The average hardness value of this sample, noted down before the error, correlated with other web measurements.

In order to evaluate the steel's mechanical properties, a combined approach using the ISO 18265 and PN-H-04357 standards [34] was implemented. This involved using the HV10 values to calculate the tensile strength, or R_{mV}, by interpolating values given in ISO 18265. Furthermore, in alignment with the PN-H-04357:1993 standard, a consistent ratio of $\alpha = R_{eV}/R_{mV}$, set at 0.7, was used for each tested component of the steel bridge to determine the yield strength.

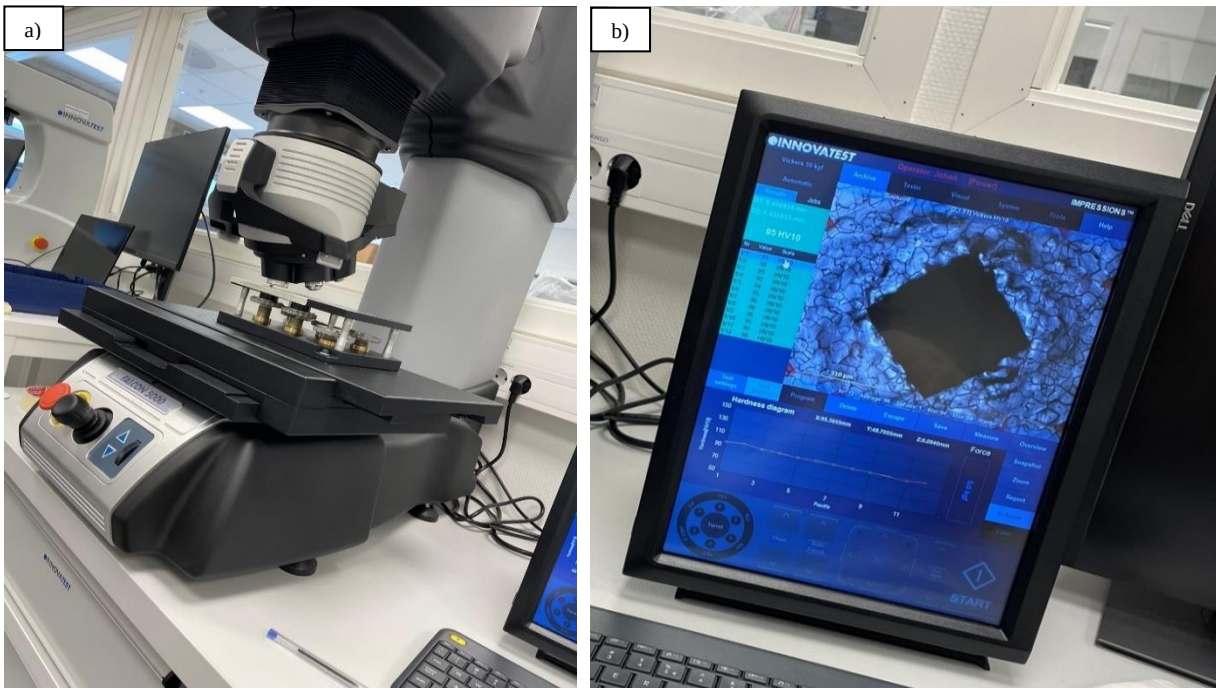

Figure 11: The fully automated hardness tester Falcon 5000 a) and built-in software from Innovatest showing the image of a single indentation b)

3.2.5 Experimental buckling testing

The theoretical calculations were conducted using Eurocode 3 as the foundational standard for determining the design moment resistance of the structural element. The load arrangement for each beam was experimentally determined, see Figure 13. Initial tests on Beam 1 used a four-point load with variable spacing. However, this method did not yield optimal results as force applied far exceeded calculated capacity, and lateral-torsional buckling behavior were very limited. This prompted a shift to a three-point load which provided significantly better outcomes and applied to Beam 3 and 4. The calculations were executed using SAP2000, considering two sets of material properties: the acquired properties from testing, utilizing 95% characteristic values, and the values recommended for bridges of this age, specifically those of S235 steel. No safety factors were used. However, it's important to note that these calculations were somewhat simplified. The corrosion damage of the structure, which results in a loss of cross-sectional area, or the open holes once filled with rivets, located approximately at the beam's midpoint, was not considered for theoretical calculations.

For the experimental testing, each beam was cautiously lifted onto the Toni-Tech flexural strength machine, effectively secured to prevent accidental tipping, or falling. The experiment marked the debut of new instruments, specifically the strain gauges, employed to collect vital data. Additional sensors were installed to measure both deflection and lateral displacement, broadening the scope of data gathered. The test proceeded by applying a load at a rate of 20kN/min, continuing until notable buckling signs appeared on the beams, marking the successful completion of the tests.

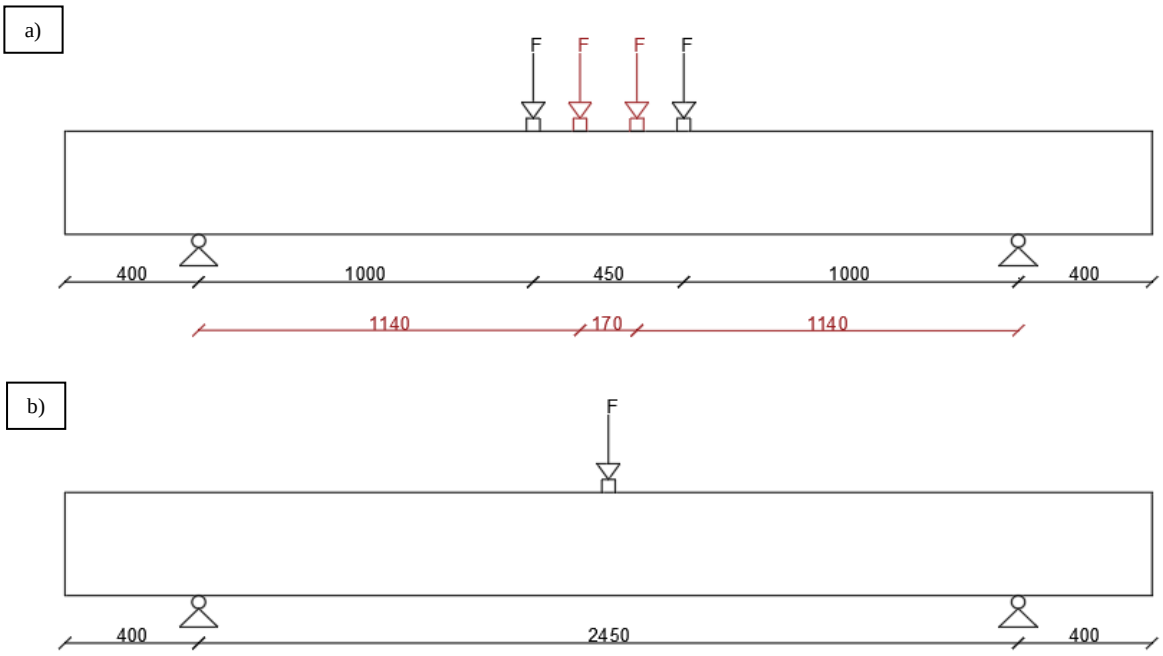

Figure 12: Schematic of beam test setup. a) Shows the four-point load applied solely to Beam 1, with the black dimensions indicating the first test run and the red dimensions indicating the second test. b) Illustrates the three-point load applied to the remaining beams, specifically Beam 3 and Beam 4.

4. Results and discussion

4.1 Chemical composition and microstructural findings

Table 12: Comparison of Beam 2's chemical analysis with nominal values from literature [2, 8, 35]

Material	Process	Chemical composition [%]				
		C	Si	Mn	P	S
Beam 2	-	0.0296	<0.0010	0.369	0.0312	0.0530
Chemical composition according to literature data						
Puddle iron [8]	-	0.032-0.15	0.003-0.42	0.054-0.11	0.011-0.39	0.0034-0.018
Mild steel [2] 19th century	Bessemer Thomas	0.02-0.10	>0.08 <0.08	0.30-0.50	0.011-0.39	0.0034-0.018
	S-M	0.05-0.15	-	0.20-0.50	0.03-0.06	0.012-0-15
Mild steel [2] 20th century	Thomas & S-M	0-10-0.20	0.01	0.40-0.50		
Rimmed steel [8]	-	0.026-0.20	0.001-0.013	0.036-0.52	0.009-0.136	0.063-0.176
S235 [35]	-	<0.17	-	<1.40	<0.045	<0.045

S-M: Siemens-Martin process
Mild steel, also known as rimmed steel [8]

Chemical analysis results for the aged steel beam, as presented in Table 12, align closely with the literature data for mild steel. This classification is made based on the beam's composition, which showcases heightened levels of manganese and sulfur, and limited silicon content - a profile more indicative of mild steel rather than puddle iron. Additionally, the low carbon content in comparison to modern mild steel hints at an early 1900s fabrication date. This interpretation is further supported by the findings of Cremona et al. [3], according to whom, puddle (wrought) iron was prevalent until 1900, while mild steel became the preferred choice from the late 1890s to the 1920s. Therefore, the examined steel beam can likely be characterized as mild steel.

With a sulfur content of 0.00530%, Beam 2 considerably exceeds the typical values associated with the Bessemer and Thomas processes. This anomaly suggests a potential production through the Siemens-Martin process, which is known for yielding steel with higher sulfur content [3]. The marked variations in the chemical compositions of both puddle iron and mild steel, as indicated in Table x, underscore the lack of standardization in steelmaking practices of that time. Manufacturers followed their own unique practices and formulas, adding to the difficulty in definitively distinguishing between converter steels, such as Thomas steel, and the

relatively purer Siemens-Martin steels. Patterns showcased in Figure 15 resemble sulfur imprints common in puddled iron (as seen in Helmereich et al. [8]), but these only appear in polished samples. However, this comparison invites a significant degree of uncertainty, given the absence of the Baumann method's application to these epoxy-encased samples.

A relatively uniform, all-ferritic steel microstructure was observed under the microscope distinguished by clear boundaries separating the ferrite grains and a generally equiaxed grain formation. Non-metallic inclusions are visible in all areas of the cross-section. These rather small darker areas, subjected to an Energy-Dispersive X-ray Spectroscopy (EDS), disclosed a significant presence of manganese, with smaller amounts of sulphur (refer to EDS report in Appendix B), indicating they are manganese sulfides, remnants of slag, given manganese's common occurrence in slag. Notably, the alignment of these elongated inclusions often matches the structure characteristic of the steel's rolling process. Furthermore, a specific type of inclusion, likely iron oxide, was exclusively detected in the web section of the beam. In Figure 14, one can observe one of many mechanically-induced features – a segregation band that presents itself with deformed grains coupled with an increased concentration of non-metallic inclusions situated within it. The microstructure exhibits marked similarity to the mild steel showed in Figure 4 of Helmereich et al.'s report.

Microstructural analysis reveals the average grain size (expressed as equivalent diameter) to be approximately 28 ± 4 μm. The inclusions' composition shows miniscule deviation, with a proportion of around 2.1% ± 0.04%. Contrarily, S235, the recommended modern mild steel variant for steel produced prior to 1920, is reported to possess a smaller average grain size of 12 ± 3 μm and comprises of approximately 18% perlite within its ferritic matrix [36]. As a result, the inspected specimens display a microstructure characterized by coarser ferrite grains and an abundance of elongated non-metallic inclusions in comparison to S235. Microstructural images in Figure 14 a)-c) closely resemble those of mild steel, as presented in Helmereich et al.’s report [8]. It is important to note that these larger grains and phase inclusions can undermine the mechanical properties of ferrous alloys, impacting properties like fracture toughness, a topic to be elaborated on in subsequent sections of this thesis [36].

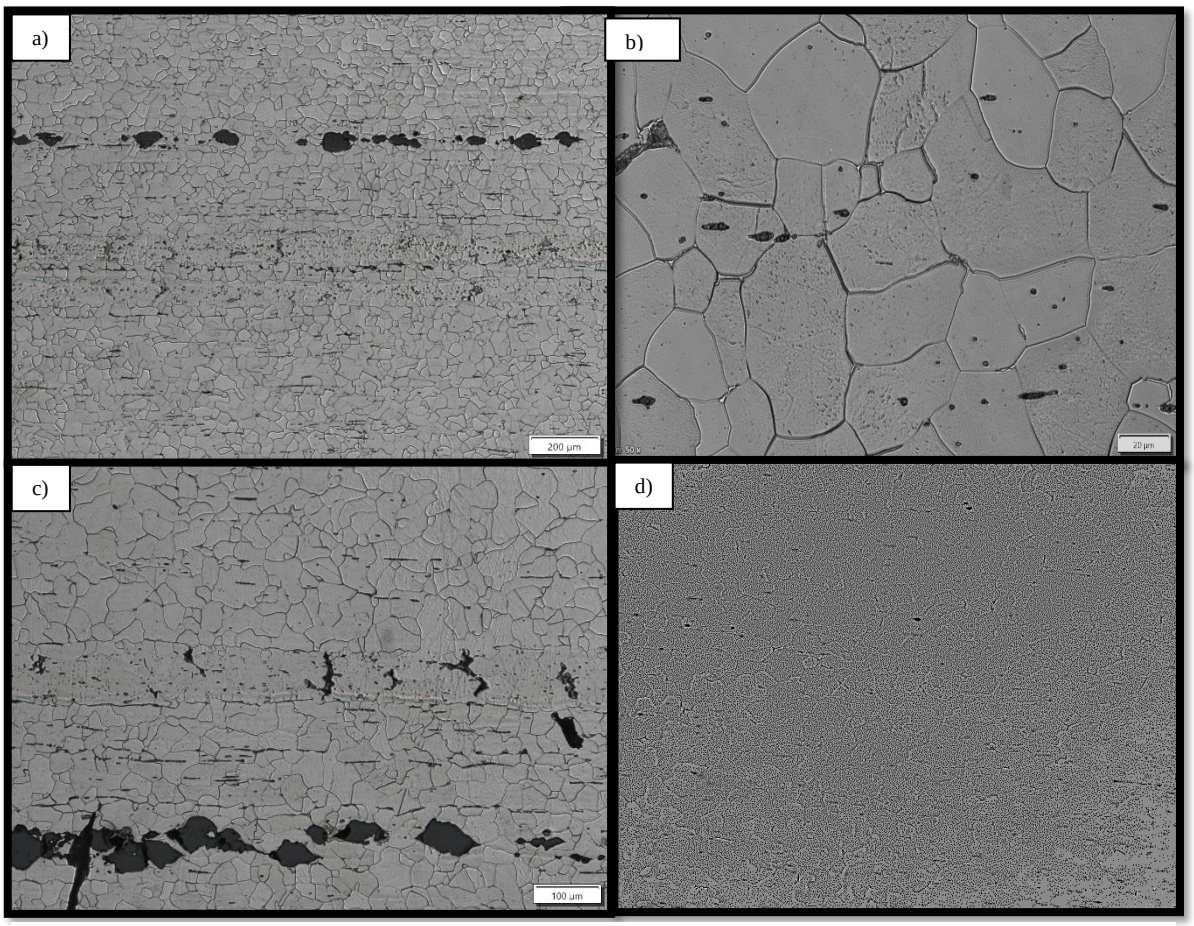

Figure 13: Metallographic test images: Microstructure of etched samples a) to c), and d) 200x magnification of grain structure without etching.

Weldability

When dealing with old steel structures, factors such as toughness and weldability warrant significant attention according to previous study on the topic [36], regardless of chemical composition. Particularly true regarding attributes such as resistance to hot and cold cracking. Weldability coefficients were ascertained through a spectrometric chemical analysis conducted by KIWA and these findings are presented in Table 13.

With the exception of the value determined from HSC, all values fall within the permissible values previously reported in literature [36]. The carbon equivalent (Ce) of the steel was 0.099, significantly below the allowable value of 0.410, indicating the steel's high weldability. A lower Ce typically suggests less chance of hardness and cracking when the steel is welded. This observation aligns with the data reported in literature by Kowal and Szala concerning other old railway structures [36]. Resistance to the formation of cold cracks during the welding process was prominently observed in the bridge steel. Conversely, a tendency for hot crack development was noted due to an HSC exceeding 4% and a Mn/S ratio in proximity to the critical lower limit of 5. This suggests the potential for an insufficient presence of manganese to bind all sulfur, thereby leading to the formation of brittle iron sulfide inclusions.

Table 13: Results from weldability calculations

Sample location	Weldability coefficients					
	C_e	HSC	C_e´	HV_{max}´	HV_{max}	Mn/S
Beam 2	0.099	5.36	0.156	UE	150.4	6.96
Permissible values	**≤ 0.410**	**< 4.00**	**< 0.400**	**< 300 HV**	**< 350 HV**	**≈ 22**

UE, underestimated value
Mn/S, ratio of manganese to sulphur content

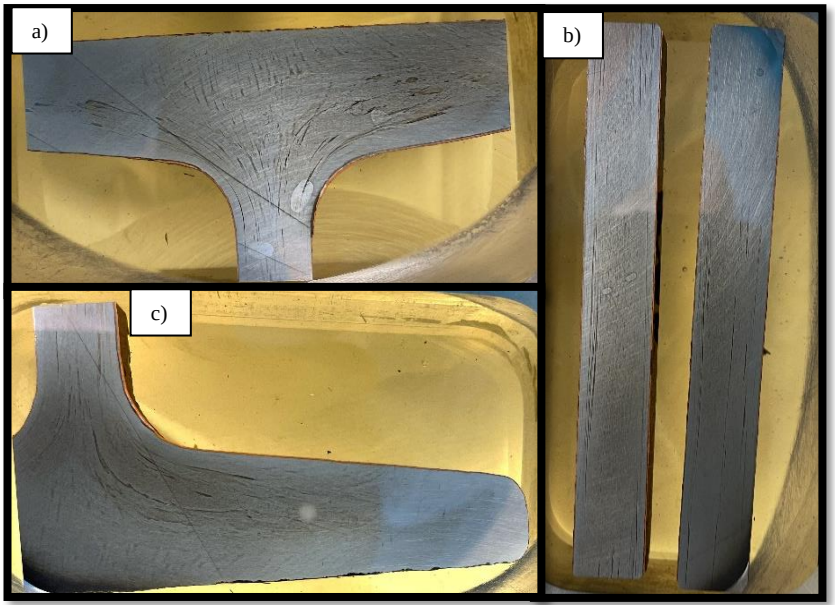

Figure 14: Images of the top flange a), web b), and bottom flange c), each encased in epoxy resin. The preparation process is incomplete due to complications encountered during the grinding and polishing stages, therefore lacking additional results.

4.2 Tensile strength outcomes

The findings from the tension tests performed on the six specimen groups are illustrated as stress-strain curves in Figure 16 and 17. Furthermore, the constructed diagrams for the samples bear a resemblance to the standard stress-strain curves obtained for modern S235 steel. These curves, featured in graphs a)-f), vary considerably - from presenting a distinct yield plateau in one instance, to the absence of a clear elastic limit in another. Given the challenge in precisely determining the upper yield point from the stress-strain diagram in all cases, employing the 0.2% offset yield method will provide a more accurate representation overall.

Table 14: Mechanical properties of tensile test samples

Specimen (1)	E [GPa]	$R_{p0,2}$ [MPa]	R_m [MPa]	A_t [%]	R_{eL} [MPa]	R_{eH} [MPa]	R_{eH}/R_m [-]
2,1 T (2)	199	241	335	37.8	248	265	0.79
2,1 B (2)	200	223	320	36.8	222	237	0.74
2,2 T	198	219	311	38.5	220	243	0.78
2,2 V	197	229	321	32.7	229	238	0.74
2,2 H	203	234	324	35.4	225	232	0.72
2,2 B	201	224	327	40.0	224	246	0.75
Mean (3)	**200**	**229**	**323**	**36.4**	**229**	**244**	0.75
Min (3)	187.7	217.4	310.3	32.2	216.1	230.9	0.72
Max (3)	208.3	245.3	335.8	40.0	269.7	284.3	0.79
SD (3)	6.2	8.5	7.7	2.6	13.0	13.6	0.026
95% (3)	189	218	311	32.4	217	232	0.752

(1) Mean values from at least 3 test samples for each specimen.

(2) Only specimens that did not experience complete destruction of samples, stayed intact.

(3) Mean, min, max, standard deviation, 95% characteristic value, are all gathered solely from the valid tensile tests (19/22).

Observations reveal that the higher yield point (ReH) ranges between 230.9 and 284.3 MPa, while the lower yield point (R_{eL}) varies from 216 to 269.7 MPa. Average R_{eL} of 229 MPa is identical to that of mild steel from old German bridges [6, 8], same is true for $R_{p0,2}$. The yield strength ratio, a measure of strain hardening up to the tensile strength, was calculated as 0.75 based on the mean value of all tests. The yield strength ratio, varying with grain size, exceeds 0.9 for modern fine-grain steels while it can be as low as 0.6 for coarse grains. In comparison, older steels generally exhibit a lower yield strength ratio, ranging from 0.6 to 0.8 [6], aligning with the ratio calculated. Ultimate tensile strength (R_m) of the specimens seems to have shown consistent values, situated within a relatively narrow range. Specifically, R_m values fluctuated between 310.3 MPa and 335.8 MPa.

Utilizing the 0.2% offset yield strength method, an average yield strength ($R_{p0,2}$) of 229 MPa was determined from all valid tensile tests. Based on the presented data in Table 14, there is a noticeable discrepancy in the yield and tensile values for the 2,1 T specimen compared to other sections of the beam. This instance stands out as it deviates from the general pattern observed in other areas of the span and cross-section. The top flange exhibits the most pronounced variance in yield strength ($R_{p0,2}$), with the 2,1 T specimen at the beam's end showcasing the highest yield strength (241 MPa) and the 2,2 T specimen at the beam's middle showing the lowest (219 MPa), suggesting potential spatial differences in material properties possibly due to factors like stress concentrations or manufacturing inconsistencies.

The 95% characteristic value of the old bridge material is compared with the standards of modern S235 steel grade, which are 235 MPa for yield strength, 370 MPa for tensile strength, and 210 GPa for E-modulus. The old material displays a yield strength of 218 MPa and a tensile strength of 311 MPa, falling short of the S235 requirements by 7.3% and 16% respectively. Its E-modulus, though lower at 189 GPa, closely aligns with the standard given the usual disregard for variations within a 5-10% range in engineering practice. This brings the E-modulus value in line with the 200 GPa guideline proposed by the International Union of Railways (UIC), emphasizing the minimal contribution of such variations to error [29].

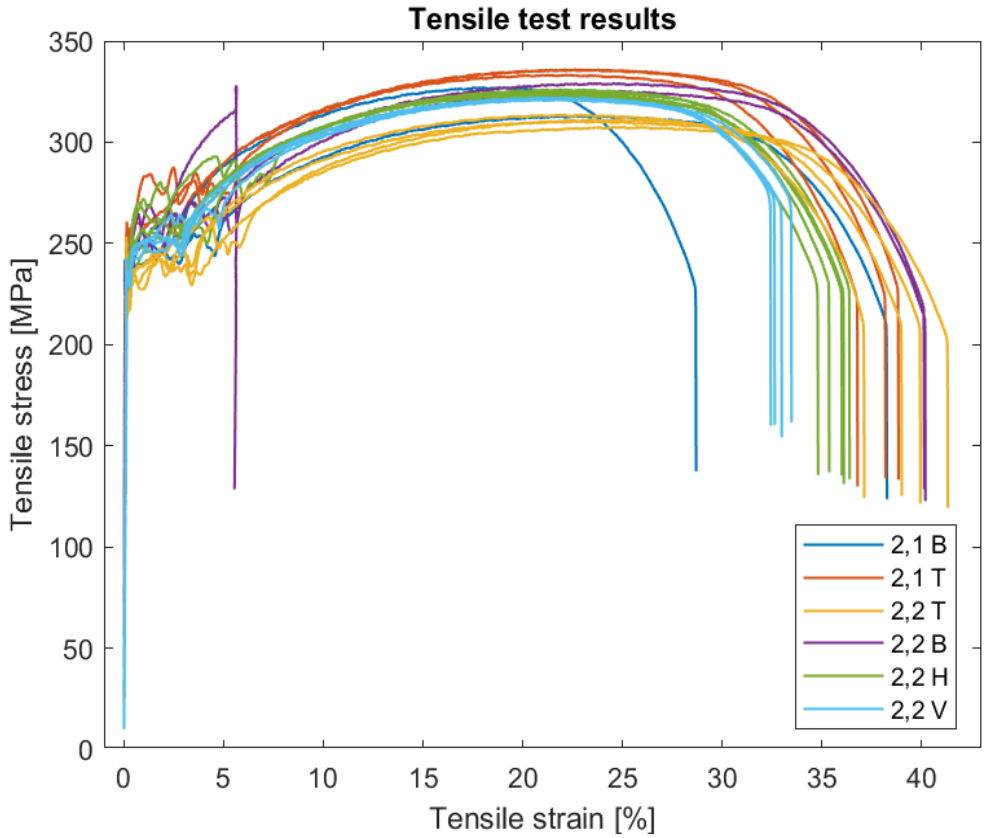

Figure 15: Results of all tensile tests with designated color according to location, including three tests deemed non-valid. Two of these outliers are notably deviating from the general trend.

Sample orientation, specifically between longitudinal and transverse samples retrieved from the web, seems to exhibit negligible influence on the measured values. This contradicts initial assumptions, given the elongated manganese sulfides observed in the microstructure generally contribute to anisotropy in mechanical properties and greatly influence the material's directional characteristics [38]. However, a 7.6% variance in ductility was detected in the longitudinal samples, marking the most substantial difference noted among the recorded properties.

The test results for the old steel generally corresponds to the reference values provided in the integrated research project "Sustainable Bridges - Assessment for Future Traffic Demands and Longer Life," for cases of old steels where no previous material data is available. The mean values for yield strength, ultimate tensile strength, and Young's modulus closely align with these reference standards. However, the material exhibits an enhanced ductility, with the elongation measurement presenting a higher value (36.36%) compared to the minimum reference range (20-25%) [1].

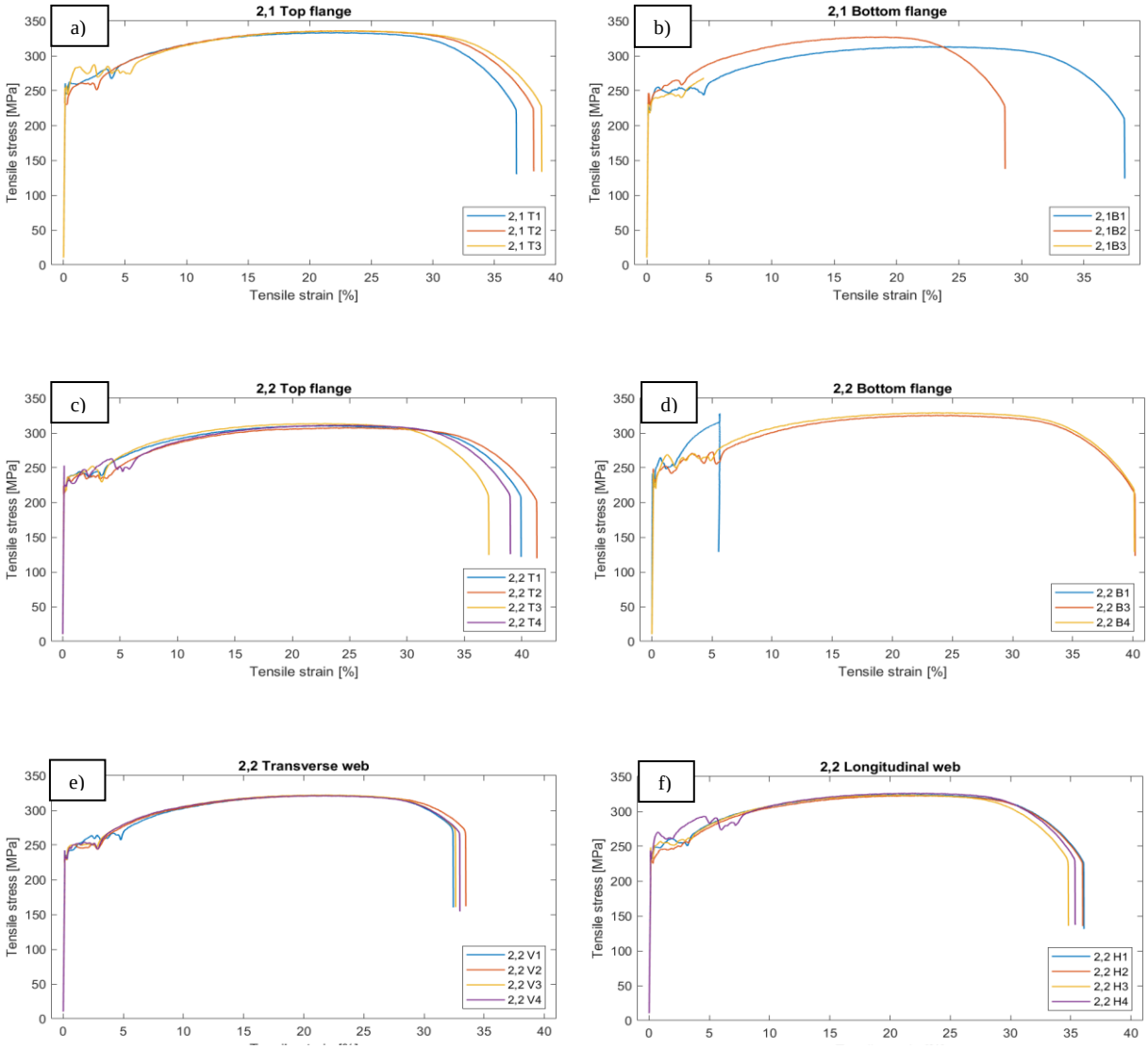

Figure 16: Stress-strain curves derived from various locations across the span and cross-section of the beam, represented in subfigures a) through f)

4.3 Impact strength evaluation

Impact tests were carried out on samples from the beam's end and middle span, at their respective flanges and web. These tests were performed at three different temperatures: +20°C, 0°C, and -20°C. The results of these 36 tests are presented in Table 15.

Table 15: Impact toughness results at various temperatures

Specimen [1]	Impact energy, KV_2 [J]		
	+20°C	0°C	-20°C
2,1 T	15.3	7.3	6.1
2,1 B	-	-	-
2,2 T	14.0	7.3	4.9
2,2 W	11.6	6.5	5.23
2,2 B	14.7	6.8	4.8
Mean [2]	**13.9**	**7.0**	**5.2**
SD [2]	2.30	0.64	0.86

[1] mean values from 3 test samples for each specimen.

[2] calculated with the respect to all test samples to each designated test temperature.

The outcome of the tests conducted on the 115-year-old steel suggests a considerably diminished impact toughness. This falls significantly short of the requirements stipulated for modern steel grades in the EN-NS 10025 standard, specifically the required value of 27J [13]. Examining the mean values derived at different temperatures, it is observed that at 20°C, the steel demonstrates its highest impact energy. However, this figure amounts to only 51.4% of the required 27J. Furthermore, at -20°C, the material lacks a staggering 80.7% of the impact energy needed to meet the criteria for the J2 designation. Of note, Eurocode 3 specifies -20°C as the requisite temperature for steel bridges of a thickness equal to or less than 30mm, along with the specified impact energy of 27J. This standard is only applicable for new structures being constructed.

The material's evident brittleness has a marked effect on its performance. Interestingly, samples extracted from the beam's web exhibited a significantly lower value compared to other parts of its cross-section. The presence of iron oxides and inclusions within the banded structures seems to affect the steel's resistance to impact. This is further compounded by the high sulfur content associated with MnS inclusions, which are known to reduce the material's resilience to brittle fractures [38]. Its low carbon content (0.0296%) could also be a contributing factor. Specifically, when carbon concentration in such early-stage steel falls below 0.10%, it tends to age more quickly, a process often linked to increased brittleness [29]. Despite these factors, the

brittleness level is still higher than acceptable, pointing to additional influences or conditions that warrant further investigation.

While a complete impact vs. temperature curve could not be plotted due to the low impact energy of the samples, research suggests the transition temperature for old mild steels to be within the 0 to 40 °C range [39]. The transition temperature, while informative, holds lesser relevance in Norway's colder climate, where the steel predominantly functions within its brittle state. The primary interest lies in the energy absorption at the lowest probable temperature that the structure would encounter, which in Norway, is expected to be below 0 degrees. Even so, it should be noted that the energy absorption remains quite low until the temperature rises to 20 °C.

In total, 36 samples were subjected to testing, with each test consistently resulting in a complete fracture, with the material incapable of withstanding the imposed impact. These results further underline the significant differences in material properties between this historic steel and modern steel grade given in V413 [25].

Visual inspection of the sample's fracture surface post-testing displayed a lustrous, "crystalline" appearance (Figure 18 a)), signifying the occurrence of cleavage – a mode of fracture where atomic separation occurs along specific lines of crystallographic planes [40]. The sample is displaying no evidence of ductile deformation, such as necking or elongation.

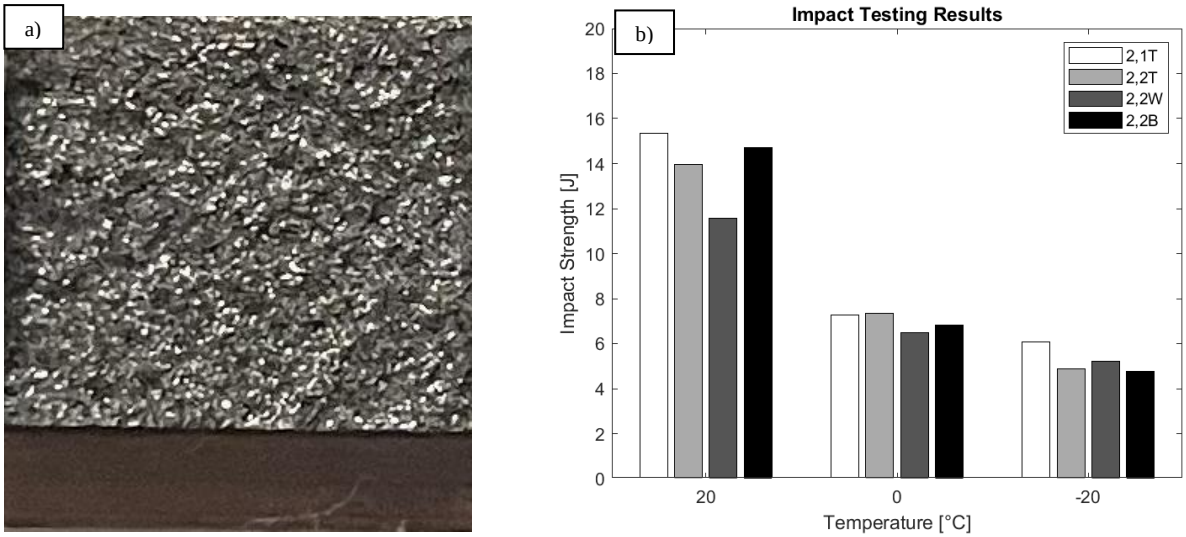

Figure 17: a) A visual representation of the fracture surface following an impact test, representative for all test samples. b) Results of the impact test, differentiated by color corresponding to the location at each test temperature.

Typically, steel demonstrates a clear shift in fracture mechanism with temperature changes, moving from ductile to brittle as temperature decreases. However, the Scanning Electron Microscopy (SEM) analyses of fracture surfaces across various temperatures (shown in Fig. 19) reveal a consistent fracture pattern. These findings suggest that the old steel exhibits a dominance of brittle fracture (cleavage) across the tested temperature range. The materials' low ductility, particularly notable perpendicular to the rolling direction, is further

demonstrated through the observed lamellar tearing and elongated flat inclusions seen at 20°C, as evidenced in Figure 19 a). Throughout the entire temperature spectrum tested, a prominent river-like pattern is evident, instigated by cracking initiated at the grain boundaries. This is indicative of a cleavage fracture, a type of brittle failure. Curiously, the presence of shallow dimples, usually suggestive of some ductile behavior, was also found across all temperatures, but overall miniscule signs of this type of behavior. These observations, coupled with the consistently brittle fracture pattern, raise concerns about the old steel's toughness, potentially affecting the structural integrity and durability of structures composed of similar material.

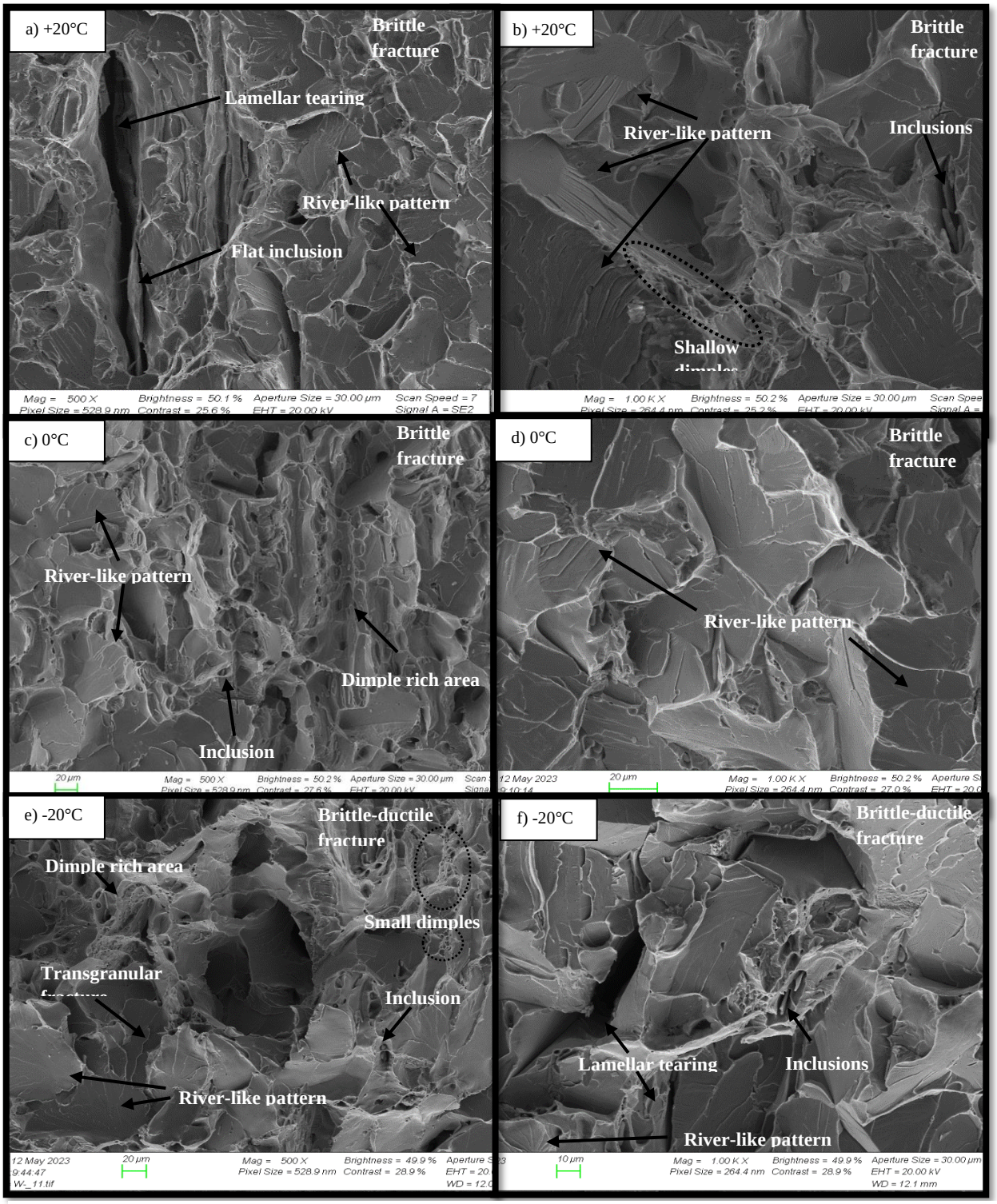

Figure 18: Fracture development with decreasing temperature from +20°C to -20°C. Mag = 500x and 1000x

4.4 Hardness test results

Table 16: Assessment of material hardness, determination of estimated mechanical properties, and comparison of estimated parameters with measured values in Table 14

Location	Hardness, HV10			R_{eV} [MPa]	R_{mV} [MPa]	$\frac{R_e}{R_{eV}}$	$\frac{R_m}{R_{mV}}$
	Average	SD	CV				
Top flange	93.1	2,92	88.3	207	296	1.10	1.08
Web	100.0	4.07	93.3	228	326	0.99	0.97
Bottom flange	94.0	3.33	88.5	206	294	1.09	1.05
Cross-section	**95.4**	**4.51**	**88.0**	**216**	**308**	**1.05**	**1.04**

R_{eV} – estimation of yield strength derived from Vickers hardness

R_{mV} – estimation of ultimate tensile strength derived from Vickers hardness

The hardness values of the examined steel, with an average of 95.4 HV10, are noticeably lower when compared with those of modern structural steel grades such as S235 (128 HV10) and S355 (155 HV10) [36]. The hardness observed in the beam's web appears to be marginally greater than that in its flanges, displaying a slight difference of approximately 6-7%. These lower hardness values can likely be ascribed to the steel's low carbon content and coarser grain structure, differing from modern low carbon steels. Typically, greater hardness and improved mechanical properties are associated with higher carbon content and finer grains. In line with these findings, the Sustainable Bridges report proposes similar Charpy V-Notch values [1] and highlights that the materials used in historic bridges tend to exhibit more brittle characteristics compared to their modern equivalents [41].

Given the positive correlation between hardness values and tensile strength, it is feasible to establish empirical relationships for specific applications. By employing both ISO 18265 and PN-H-04357 standards [34], an assessment of the steel's mechanical properties was conducted. The findings aligned closely with data from the tensile tests, as seen in figure x, thereby indicating an interesting approach for material analysis. However, it should be noted that the yield and tensile strength for the top and bottom flanges were slightly overestimated, exceeding the actual values by 5% to 10%. On the other hand, a negligible underestimation was observed in the case of the web samples. In scenarios where for instance only hardness values can be obtained, this method can provide a useful indication of a material's yield and ultimate strength.

4.5 Comparing theoretical and experimental buckling results

It is showcased in Table 17 the differences between theoretical predictions and experimental findings related to the lateral-torsional buckling moment capacities of three tested beams.

Table 17: Theoretical and experimental values

	Theoretical values		Experimental values
	$M_{b,Rd}$* [kNm]	$M_{b,Rd}$ [kNm]	Max bending moment [kNm]
Beam 1, test one	139.2	138.8	197.5
Beam 1, test two	139.2	138.8	225.2
Beam 3	145,4	145.0	175.2
Beam 4	145.4	145.0	195.4

$M_{b,Rd}$: Lateral-torsional buckling moment capacity
*using material properties acquired from tensile testing

The theoretical estimates, whether based on tensile testing data or material properties of S235 mat, were consistently lower than the experimentally determined maximum bending moments. This implies that these beams could endure greater loads than initially estimated, underscoring their resilience in real-world conditions. As illustrated in Figure 20, the buckling behavior starts to appear at values exceeding 200 kN, significantly higher than those predicted theoretically.

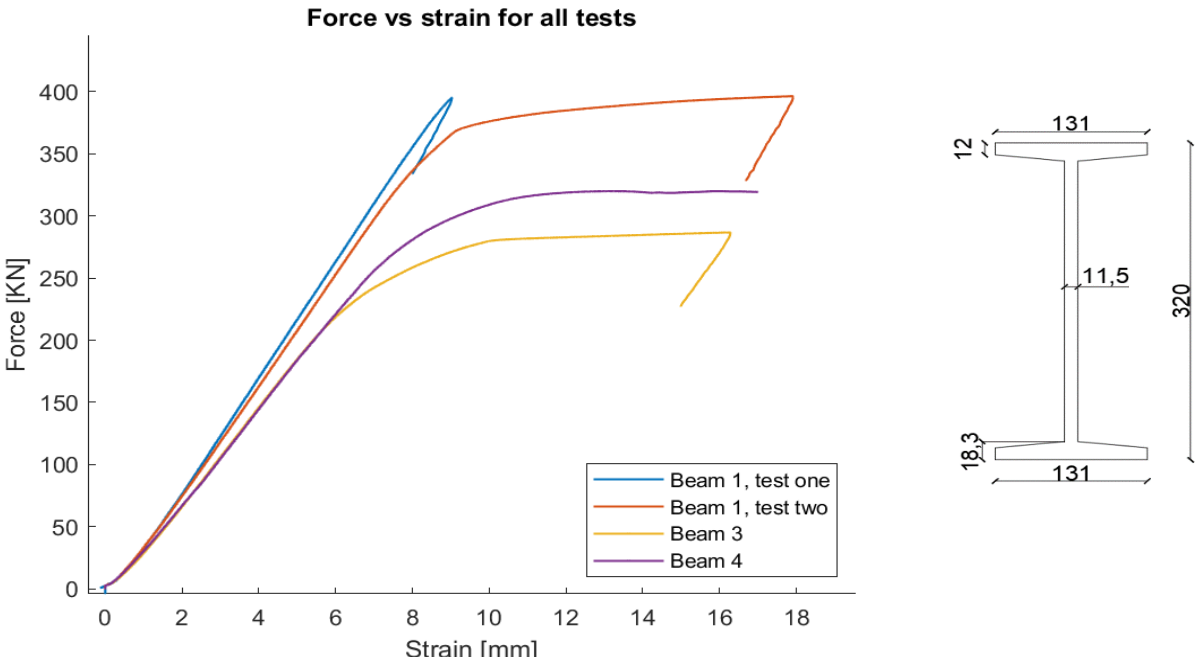

Figure 19: Force vs strain for all buckling tests performed on the individual beams with cross-section on the right side.

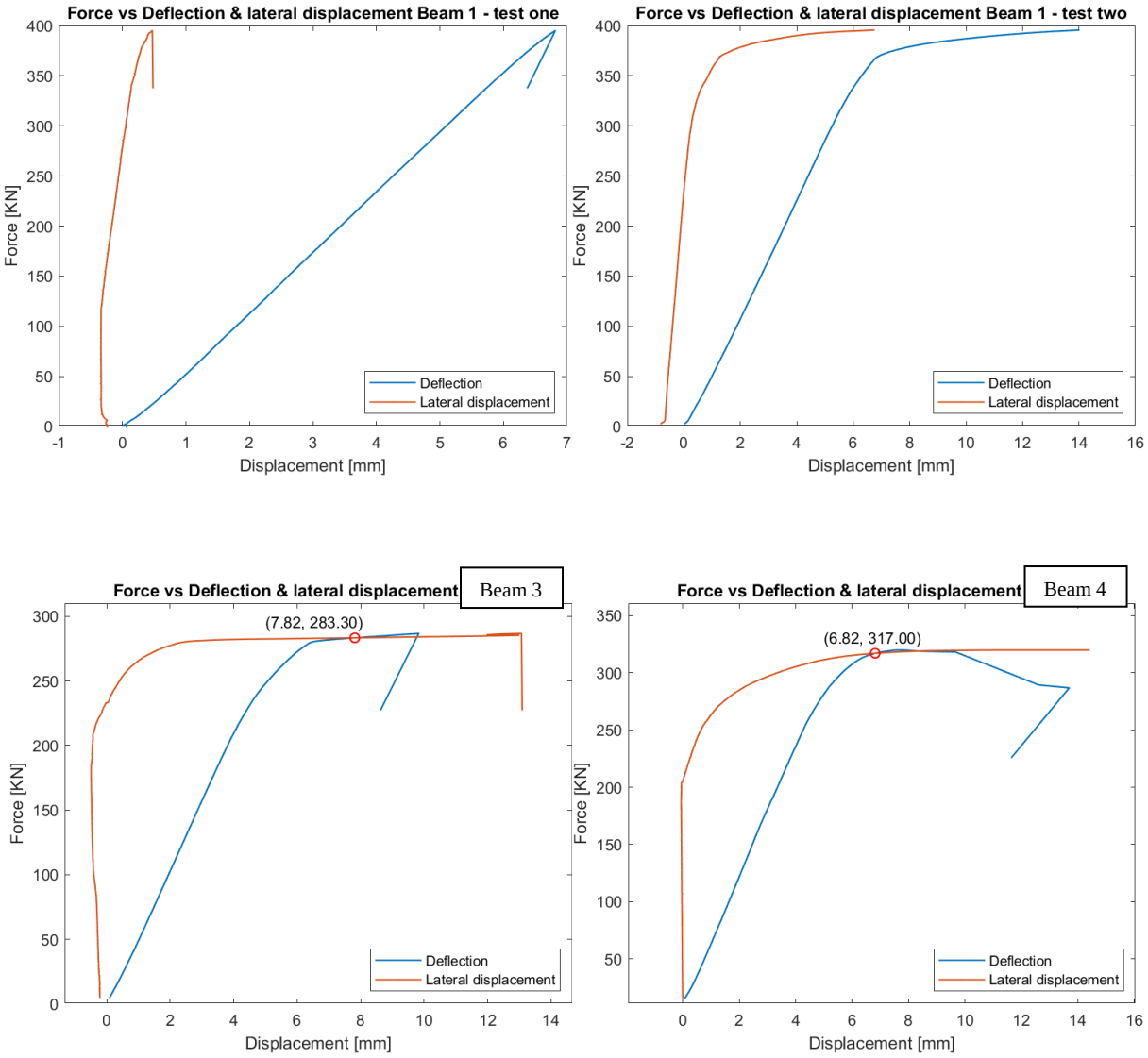

Figure 20: Graphical representation of force as a function of both deflection and measured lateral displacement for the specified beam

Experimental results obtained from testing Beams 3 and 4 suggest that the intersection of deflection and lateral displacement (as illustrated in Figure 21) provides an indication as to when lateral-torsional behavior (LTB) begins, where it bends laterally and twist about its longitudinal axis. A notable difference is apparent in the intersection points: (7.82mm displacement, 283.3kN) and (6.82mm displacement, 317.0kN), demonstrating over a 10% variation in values. As displayed in Figure 22 b), global buckling, which all three beams experienced, becomes evident.

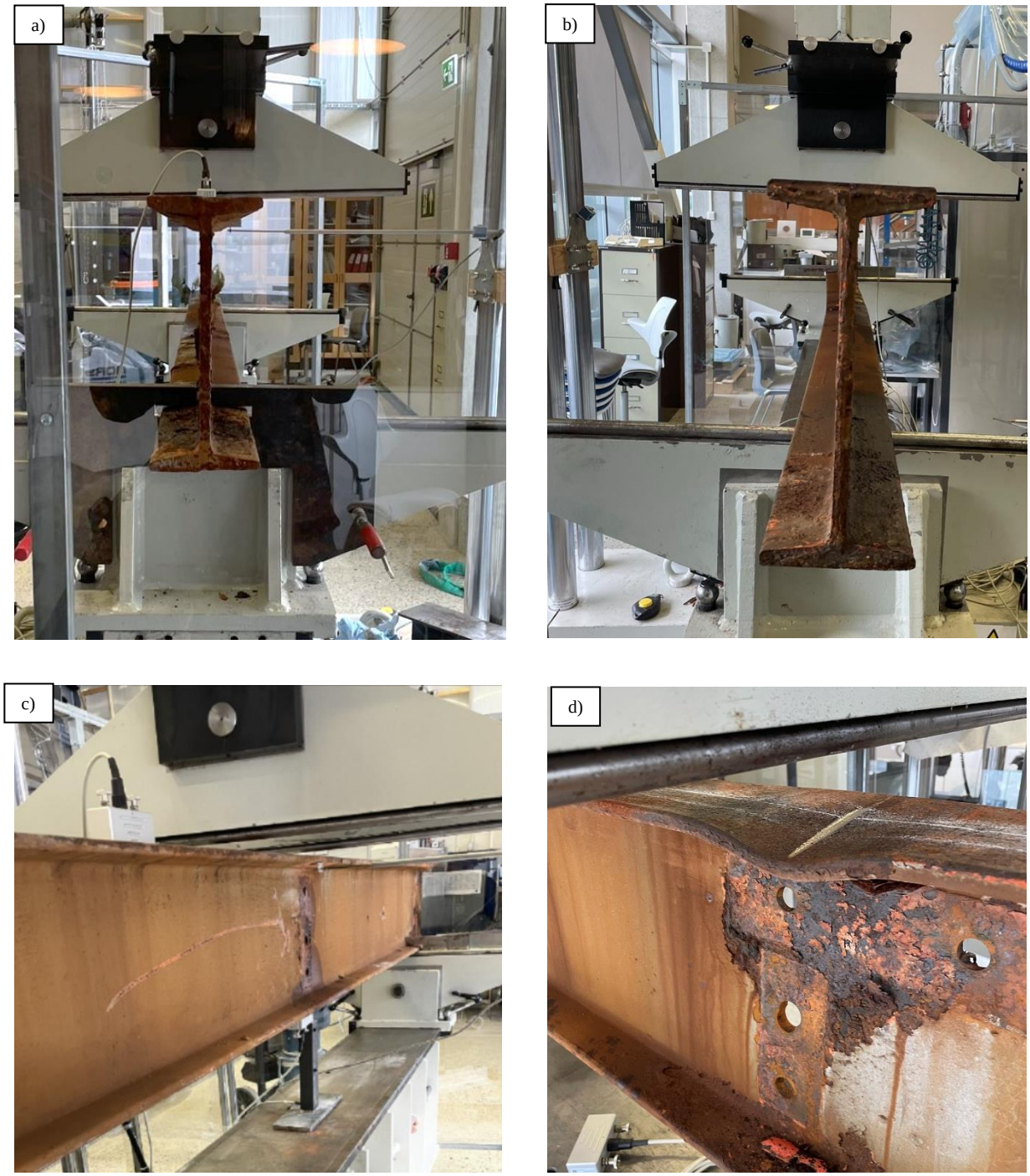

Figure 21: a) Beam setup before the buckling test, showcasing the rod for measuring lateral displacement. b) Post-test condition of the beam. c) Close-up of the beam with top and bottom strain gauges adjacent to the deflection sensor. d) The resultant damage.

5. Conclusions and future work

This pilot project offers a comprehensive examination of the mechanical and microstructural attributes of steel components from a bridge over 100 years old originating from a Norwegian smelt plant. The outcomes were compared with the characteristics of both materials of the construction period and modern structural steel. Given the bridge's age, its exposure to the elements, and production methods at the time, it is not unexpected that most mechanical properties diverge from modern structural steel, specifically S235. However, while not fully meeting S235 standards, the yield strength and ductility remain notably robust, falling more in line with the standards proposed by the UIC. Based on the mechanical properties, the reasoning behind the structure's demolition becomes evident. Despite this, it remained possible for the bridge to continue serving its purpose. But this would have required new structural analyses, the implementation of necessary strengthening measures, adaptations to meet evolving infrastructure demands, as well as regular maintenance. Regardless, any attempt to work with early steels should begin with a thorough understanding of their properties to ensure the feasibility of the desired operations.

1. Chemical analysis of the aged steel beam reveals a composition characterized by elevated levels of manganese and sulfur, alongside limited silicon and low carbon content. Additionally, microscopic examination confirms a coarse-grained, polygonal ferritic structure, with the presence of non-metallic inclusions and oxides. This closely mirrors the mild steel profile depicted in the literature. It is important to note that during the bridge's construction in 1908, mild steel had already been well-established as the preferred material for steel structures. Taken together, these observations affirm the beam's material as mild steel. The notably high sulfur content further suggests that its production method may have been the Siemens-Martin process. However, given the unique manufacturing practices of the time and variability in material composition reported in literature, a certain level of uncertainty remains.
2. Spectrometric analysis results were utilized to assess the weldability of the examined steel. The obtained values, being lower than the critical thresholds established in existing literature, indicate that the steel is weldable. However, for absolute certainty, more comprehensive methods like cold-cracking tests might be necessary. These findings propose that the steel beams could potentially be reinforced using classical repair methods, such as increasing the cross-section by welding.
3. The steel samples from the tensile tests revealed a yield strength (f_y) of 218 MPa and an ultimate tensile strength (f_u) of 311 MPa, demonstrating good ductility with an elongation (A_t) equal to 32.4%. While these values do not fully meet the requirements of S235, a steel grade currently used in Norwegian bridge construction that requires $f_y \geq 235$ MPa, $f_u \geq 370$ MPa, and $A_t \geq 26\%$, they align well with the standards proposed by the UIC, specifically $f_y = 220$ MPa and $f_u = 320–380$ MPa. Notably, the influence of sample orientation on the anisotropy of the properties was found to be minimal. It is worth noting that the stress-strain diagrams from the tests generally lack a clear elastic limit, which distinguishes them from those typical of modern steel.

4. Impact strength of the studied 115-year-old steel beam falls significantly short of modern standards (EN-NS 10025), with readings 50-81% below the required 27J across all tested temperatures (+20°C, 0°C, and -20°C). Notably, the steel exhibits especially diminished toughness at lower temperatures. Samples from web shows lower values, attributed to the presence of iron oxides, inclusions, high sulfur content, and low carbon content contributing to increased brittleness. This brittleness was further underscored by SEM images, which revealed predominantly cleavage fractures with characteristic river-like patterns.
5. With an average hardness of 95.4 HV10, the steel under investigation significantly underperforms modern structural steel types in terms of hardness. This lower hardness is likely due to the material's low carbon content and coarse grain structure. Marginal variations were observed in relation to location within the cross-section, with the web area demonstrating slightly higher hardness. Despite these minor discrepancies, hardness measurements can offer valuable insights for estimating yield and tensile strengths, particularly when only hardness data is accessible.
6. As anticipated, every test conducted experienced lateral-torsional buckling behavior. The experimental results demonstrated a higher capacity than what was projected in theoretical calculations, which were carried out without the use of safety factors.

This project underscores the potential longevity of early steel structures when their properties are well-understood and appropriately managed, offering valuable insights for future restoration and preservation efforts.

Future work

Although the research conducted in this report adequately meets its stated objectives, it inevitably leaves some questions unanswered, requiring additional investigation. Below, potential topics for further exploration are suggested.

- Structural steels vary widely, with even minor variations in chemical composition or manufacturing parameters leading to significant alterations in their properties. Consequently, an examination of other structural components of the bridge would serve to deepen our understanding of the material's character.
- Previous research has reported significant impacts of inclusions and oxides on mechanical properties, dependent on orientation, either transverse or longitudinal [38]. Although no clear effect was observed in this thesis, further testing might provide additional insights.
- Fatigue testing is crucial for a comprehensive characterization of the material. Since it is one of the main causes of bridge failure, further investigation in this domain is recommended.
- Investigating the effects of heat treatments on the material, such as normalizing treatment and full annealing, would be beneficial.
- Assessment of general corrosion throughout the structure, along with a focus on areas of pitting corrosion, and its effect, could provide further crucial data.
- A more in-depth study focusing on the microstructure could be undertaken, possibly applying sulfur print to reveal the segregation lines containing phosphorus and sulphur.

7. References

[1] J. R. Casas *et al.*, “Guideline for Load and Resistance Assessment of Existing European Railway Bridges,” 2007. [Online]. Available: https://www.diva-portal.org/smash/get/diva2:1328606/FULLTEXT01.pdf

[2] Kuhn et al, “Assessment of Existing Steel Structures: Recommendations for Estimation of Remaining Fatigue Life,” 2008. [Online]. Available: https://publications.jrc.ec.europa.eu/repository/handle/JRC43401

[3] C. Cremona, A. Patron,B. Johansson, T. Larsson,B. Eichler, S. Höhler, B. Kühn, “Improved Assessment Methods for Static and Fatigue Resistance of Old Steel Railway Bridges,” 2007. [Online]. Available: http://www.diva-portal.org/smash/get/diva2:1337428/FULLTEXT01.pdf

[4] J. Bień, Ed., *Sustainable bridges: assessment for future traffic demands and longer lives*. Wrocław: Dolnośląskie Wydawnictwo Edukacyjne, 2007.

[5] J. Hołowaty and B. Wichtowski, “Properties of Structural Steels in Historical Railway Bridges by Diagnostic Tests,” *ce papers*, vol. 5, no. 4, pp. 73–78, Sep. 2022, doi: 10.1002/cepa.1730.

[6] R. Helmerich, *Alte Stähle und Stahlkonstruktionen*. in Forschungsbericht / Bundesanstalt für Materialforschung und -prüfung, no. 271. Bremerhaven: Wirtschaftsverl. NW, Verl. für Neue Wiss, 2005.

[7] L. Gallegos Mayorga, S. Sire, M. Ragueneau, and B. Plu, “Understanding the behaviour of wrought-iron riveted assemblies: manufacture and testing in France,” *Proceedings of the Institution of Civil Engineers - Engineering History and Heritage*, vol. 170, no. 2, pp. 67–79, May 2017, doi: 10.1680/jenhh.16.00020.

[8] R. Helmerich, B. Kühn, and A. Nussbaumer, “Assessment of existing steel structures. A guideline for estimation of the remaining fatigue life,” *Structure and Infrastructure Engineering*, vol. 3, no. 3, Sep. 2007, doi: 10.1080/15732470500365562.

[9] M. Y. Demeri, *Advanced high-strength steels: science, technology, and applications*. Materials Park, Ohio: ASM International, 2013.

[10] “Metallic materials - Tensile testing Part 1: Method of test at room temperature (ISO 6892-1:2019).”

[11] J. Hołowaty, “Toughness tests on steels from old railway bridges,” *Procedia Structural Integrity*, vol. 5, pp. 1043–1050, Jan. 2017, doi: 10.1016/j.prostr.2017.07.067.

[12] Eurocode 3: Design of steel structures, “NS-EN 1993-1-1:2005+A1:204+NA:2015.”

[13] “NS-EN 10025-2:2019 - Hot rolled products of structural steels. Part 2: Technical delivery conditions for non-alloy structural steels.”

[14] N. E. Dowling, S. L. Kampe, and M. V. Kral, *Mechanical behavior of materials: engineering methods for deformation, fracture, and fatigue*, Fifth edition, Global edition. Harlow: Pearson, 2020.

[15] T. Seeger, *Stahlbau-Handbuch. 1B: Grundlagen*, 3., neu Bearb. Aufl. Köln: Stahlbau-Verl.-Ges, 1996.

[16] B. Hohlwegler, *Korrosion von Stählen aus eisernen Konstruktionen des 19. Jahrhunderts: Mineralogische und metallographische Untersuchungen an historischen Eisen und an daraus resultierenden Korrosionsprodukten.* 1993.

[17] W. Stier, D. Kosteas, and U. Graf, "Ermüdungsverhalten von Brücken aus Schweißeisens, Der Stahlbau 5," 1983.

[18] P. Langenberg, *Bruchmechanische Sicherheitsanalyse anrißgefährdeter Bauteile im Stahlbau*, Als Ms. gedr. in Berichte aus dem Institut für Eisenhüttenkunde, no. 95,14. Aachen: Shaker, 1996.

[19] F. Mang, G. Steidl, and Ö. Bucak, "„Altstahl im Bauwesen", Schweißen und Schneiden 37, Heft 1, 1989, S. 9-16."

[20] T. Beckert and A. Brand, *Hüttenkunde*. Verlag Ferdinand Ferke, Stuttgart, 1885.

[21] A. Ledebur, "Handbuch der Eisenhüttenkunde," Leipzig, 1894.

[22] K. Roesch, "Stahlerzeugungsverfahren, Deutsches Museum, Abhandlung und Berichte, 47. Jahrgang, Heft 2," 1979.

[23] Á. Paulinyi, *Das Puddeln: ein Kapitel aus der Geschichte des Eisens in der Industriellen Revolution*. in Abhandlungen und Berichte, no. n. F., Bd. 4. München: R. Oldenbourg, 1987.

[24] K. Eriksson, "Toughness requirements for older structural steels," presented at the IABSE Workshop" Remaining Fatigue Life of Steel Structures": 17/12/1990, Lausanne: International Association for Bridge and Structural Engineering, 1990, pp. 95–101.

[25] Statens Vegvesen, "V413 Bæreevneklassifisering av bruer, materialer." 2023. [Online]. Available: https://store.vegnorm.vegvesen.no/v413

[26] N. S. Trahair, Ed., *The behaviour and design of steel structures to EC3*, 4th ed. London ; New York: Taylor & Francis, 2008.

[27] European Commission. Joint Research Centre. Institute for the Protection and the Security of the Citizen., *Eurocodes, background & applications: design of steel buildings.* LU: Publications Office, 2015. [Online]. Available: https://data.europa.eu/doi/10.2788/605700

[28] "ASTM E3-11(2017), Standard Guide for Preparation of Metallographic Specimens." 2017.

[29] J. Hołowaty and B. Wichtowski, “Properties of steel in railway bridge constructed in 1887,” *Roads and Bridges - Drogi i Mosty*, vol. 14, no. 4, Art. no. 4, Jan. 2016, doi: 10.7409/rabdim.015.018.

[30] J. Pilarczyk, *Poradnik inżyniera: spawalnictwo (Polish)/Engineering handbook: welding*. 2008.

[31] J. Hołowaty and B. Wichtowski, “Welding issues in retrofitting of old railway bridges / Problemy spawalnicze przy modernizacji starych mostów kolejowych,” *Przegląd Spawalnictwa*, vol. 87, no. 5, May 2015, doi: 10.26628/ps.v87i5.225.

[32] J. C. Lippold, *Welding metallurgy and weldability*. Hoboken, New Jersey: John Wiley & Sons Inc, 2015.

[33] “Metallic materials - Charpy pendulum impact test Part 1: Test method (ISO 148-1:2016).”

[34] “ISO 18265:2013 - Metallic materials — Conversion of hardness values.”

[35] Norsk staal, “Steel Tables.”

[36] M. Kowal and M. Szala, “Diagnosis of the microstructural and mechanical properties of over century-old steel railway bridge components,” *Engineering Failure Analysis*, vol. 110, p. 104447, Mar. 2020, doi: 10.1016/j.engfailanal.2020.104447.

[37] R. Helmerich, *Alte Stähle und Stahlkonstruktionen: Materialuntersuchungen, Ermüdungsversuche an originalen Brückenträgern und Messungen von 1990 bis 2003*. in Forschungsbericht / Bundesanstalt für Materialforschung und -prüfung, no. 271. Bremerhaven: Wirtschaftsverl. NW, Verl. für Neue Wiss, 2005.

[38] G. Krauss, *Steels: Processing, Structure, and Performance*, 2nd ed. Materials Park: ASM International, 2015.

[39] L. Sieber, R. Stroetmann, H.-W. Viehrig, M. Houska, B. Vetter, and V. Schubert, *Beurteilung der Sprödbruchgefährdung gelochter Stahltragwerke: Weiterentwicklung der Analysemethoden*. in Forschungsinitiative Zukunft Bau F, no. 2972. Stuttgart: Fraunhofer IRB Verlag, 2015.

[40] T. H. Courtney, *Mechanical behavior of materials*, 2. ed. Long Grove, Illinois: Waveland Press, 2005.

[41] A. Pipinato, C. Pellegrino, O. S. Bursi, and C. Modena, “High-cycle fatigue behavior of riveted connections for railway metal bridges,” *Journal of Constructional Steel Research*, vol. 65, no. 12, pp. 2167–2175, Dec. 2009, doi: 10.1016/j.jcsr.2009.06.019.

Appendix A. Detailed chemical report

TEST REPORT

DATE OF ISSUE : 08.06.2023 REPORT NO. : 23NO-00201OR01

CUSTOMER : **Universitetet i Stavanger**
Kjell Arholms gate 41
4021 Stavanger

PROJECT : -

DESCRIPTION : **Chemical analysis of IPE steel beam**

SPECIFICATION : **NS-EN ISO 14284:2002, ASTM E415:17**

IDENTIFICATION OF TEST PIECE(S):

Material	:	Grade:	I S205G1T
Geometry	:	Thickness [mm]:	10,1
		Sample width [mm]:	22,3
		Sample length [mm]:	13,2
		Samples received:	1
		Sampling by Kiwa:	No

Date approved: 08.06.2023

Vidar Lyngmo, Technical Adviser

Kiwa
Kabelgaten 2
NO 0580 Oslo
Norway

Kiwa, location Rygge
Granheimveien 12
NO 1580 Rygge
Norway

Contact:
Phone: +47 22 88 50 00
E-mail: post.norge@kiwa.com
VAT: NO976491696MVA

Kiwa.no

Test overview

Not accredited test **TEST SPECIMENS:**

Chemical analysis: Identification: 201OR01-1

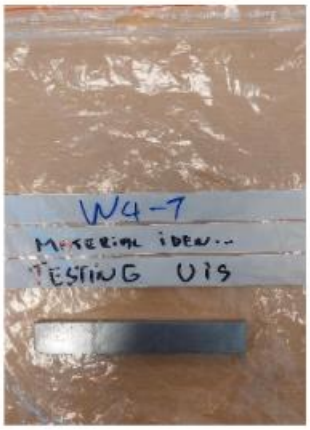

Notes:

Test specimens and remaining material will be stored for three months unless otherwise is agreed.

The testing was carried out in normal laboratory environment unless otherwise stated.

Decision rule for test results unless otherwise agreed.

Accepted / Acc.	The measurement result with uncertainty (95% confidence interval) within acceptance limit.
Accepted* / Acc.*	The measurement result within the acceptance limit, but uncertainty (95% confidence interval) measurement result may be outside acceptance limit.

Chemical analysis - Spectrometer

Type of test: **Chemical analysis of IPE steel beam**

Report No.: **23NO-00201OR01**

Customer: **Universitetet i Stavanger**

Chemical analysis

Spectrometer: Foundry Master, serial no: 44Q0066

Test standard: NS-EN ISO 14284:2002, ASTM E415:17

Reference sample identification no: BS 2931A

Test procedure No.: 3207

Test no. 201OR01-1

	Fe	C	Si	Mn	P	S	Cr	Mo
Ave	99.3	0.0296	< 0.0010	0.369	0.0312	0.0530	0.0122	0.0128

	Ni	Al	Co	Cu	Nb	Ti	V	W
Ave	0.0405	< 0.0010	0.0154	0.0085	0.0035	0.0019	0.0008	< 0.0050

	Pb	Sn	B	Ca	Zr	Zn	Bi	As
Ave	< 0.0050	0.0007	0.0003	< 0.0001	0.0018	< 0.0005	< 0.0010	0.0730

	N	Se	Sb	Ta	Pcm	CE
Ave	0.0024	< 0.0010	0.0041	0.0110	0.05	0.10

Evaluation:

The chemical composition of the specimen corresponds to a structural steel, material no. 1.0028 or 1.0032 , with a higher sulphur content than specified for the grades (alternative names DIN/EN: St 34-2, S205G1T).

Date: 30.05.2023

Performed by: Siv M. Nordtømme

Appendix B. EDS reports

EDAX TEAM

Per Kristian - Bjelke

Author: EspenU
Creation: 04/27/2023 10:15:43 AM
Sample Name: Bjelke

Area 5

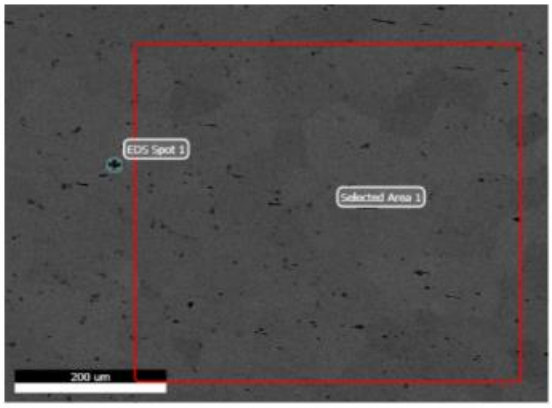

Notes:

B.1 Non-metallic inclusions

EDAX TEAM

Selected Area 1

kV:	Mag:	Takeoff:	Live Time(s):	Amp Time(µs):	Resolution:(eV)
25	500	37	100	7.68	125.8

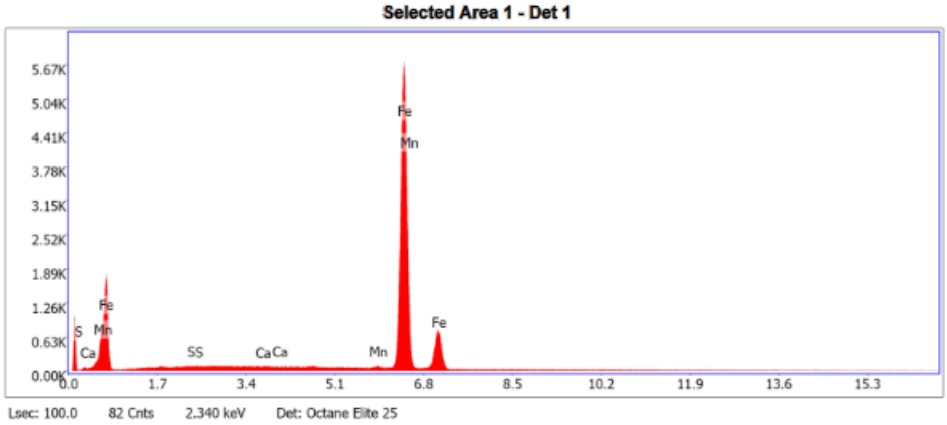

eZAF Smart Quant Results

Element	Weight %	Atomic %	Net Int.	Error %	Kratio	Z	A	F
S L	0.00	0.00	0.00	9.37	0.0000	1.1258	0.2412	1.0000
CaL	1.71	2.37	0.21	59.41	0.0131	1.0987	0.6959	1.0000
FeL	95.89	95.21	298.32	2.71	0.8184	0.9987	0.8547	1.0000
MnK	2.40	2.42	25.18	7.95	0.0269	0.9807	0.9906	1.1519

EDS Spot 1

kV:	25	Mag: 500	Takeoff: 37	Live Time(s): 100	Amp Time(µs): 7.68	Resolution:(eV) 125.8

EDS Spot 1 - Det 1

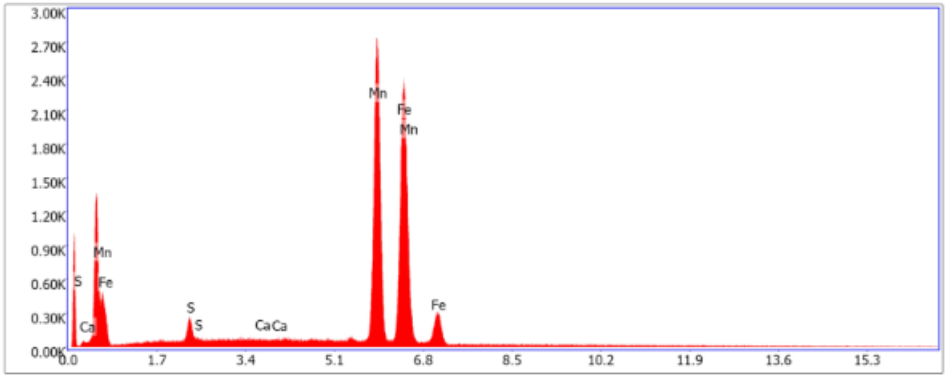

Lsec: 100.0 284 Cnts 2.340 keV Det: Octane Elite 25

eZAF Smart Quant Results

Element	Weight %	Atomic %	Net Int.	Error %	Kratio	Z	A	F
S K	1.56	2.66	31.69	13.21	0.0113	1.1476	0.6242	1.0088
CaK	0.24	0.32	4.79	43.90	0.0025	1.1153	0.8995	1.0439
MnK	55.92	55.64	796.45	1.53	0.5604	0.9895	0.9954	1.0175
FeK	42.28	41.38	543.48	1.75	0.4209	1.0075	0.9870	1.0012

B.2 Oxides

EDAX TEAM

Per Kristian - Bjelke

Author: EspenU
Creation: 05/15/2023 8:58:50 AM
Sample Name: Bjelke

Area 11

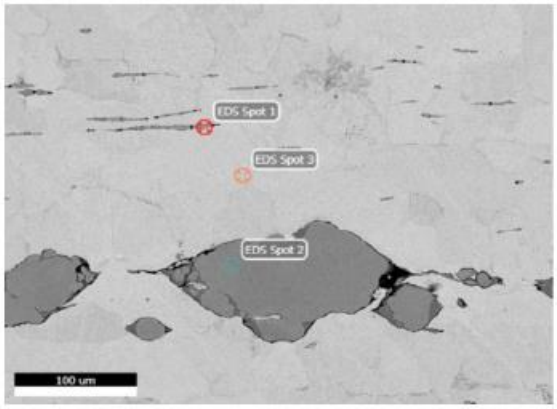

Notes:

EDS Spot 1

kV: 20 Mag:800 Takeoff: 38.1 Live Time(s): 100 Amp Time(µs):7.68 Resolution:(eV)125.8

EDS Spot 1 - Det 1

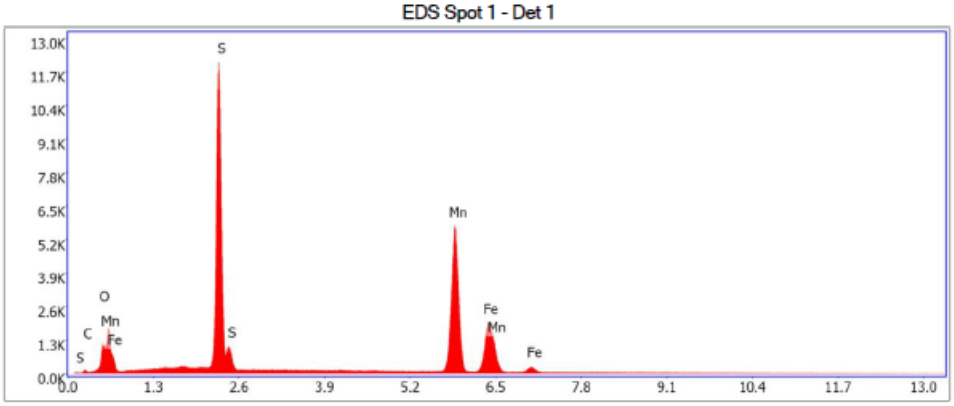

Lsec: 100.0 172 Cnts 4.150 keV Det: Octane Elite 25

eZAF Smart Quant Results

Element	Weight %	Atomic %	Net Int.	Error %	Kratio	Z	A	F
C K	0.72	2.60	3.10	47.43	0.0010	1.2695	0.1087	1.0000
O K	1.02	2.75	26.72	13.65	0.0036	1.2209	0.2868	1.0000
S K	31.41	42.31	2175.90	3.28	0.2772	1.0996	0.7983	1.0054
MnK	50.20	39.47	1530.14	1.88	0.4682	0.9391	0.9815	1.0117
FeK	16.65	12.87	452.81	2.57	0.1567	0.9549	0.9805	1.0055

EDS Spot 2

kV: 20 Mag:800 Takeoff: 38.1 Live Time(s): 100 Amp Time(µs):7.68 Resolution:(eV)125.8

EDS Spot 2 - Det 1

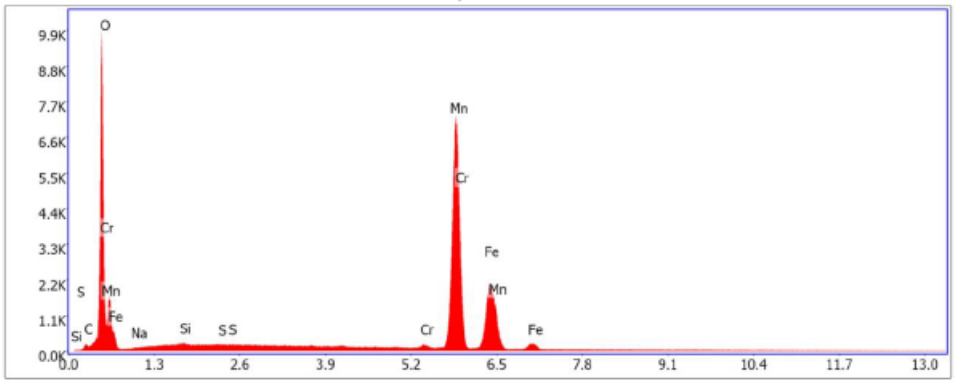

Lsec: 100.0 176 Cnts 4.150 keV Det: Octane Elite 25

eZAF Smart Quant Results

Element	Weight %	Atomic %	Net Int.	Error %	Kratio	Z	A	F
S L	0.00	0.00	0.00	37.09	0.0000	1.0795	0.2594	1.0000
C K	0.95	2.80	10.31	17.35	0.0032	1.2559	0.2699	1.0000
O K	20.85	46.29	1112.93	5.56	0.1438	1.2077	0.5712	1.0000
NaK	0.46	0.70	7.64	30.74	0.0009	1.1026	0.1757	1.0005
SiK	0.12	0.16	7.69	40.90	0.0007	1.1081	0.5354	1.0034
CrK	0.78	0.53	31.36	14.42	0.0083	0.9478	1.0004	1.1236
MnK	61.47	39.74	1951.08	1.69	0.5782	0.9286	1.0043	1.0086
FeK	15.38	9.78	432.67	2.62	0.1450	0.9442	0.9951	1.0036

EDS Spot 3

kV: 20 Mag:800 Takeoff: 38.1 Live Time(s): 100 Amp Time(µs):7.68 Resolution:(eV)125.8

EDS Spot 3 - Det 1

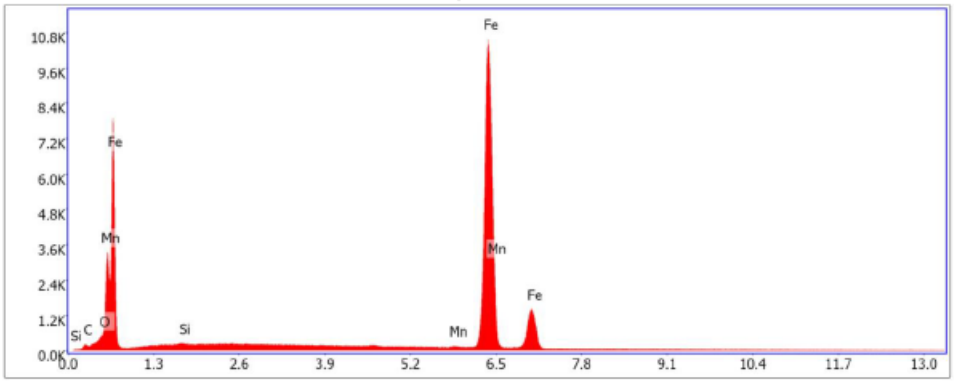

Lsec: 100.0 171 Cnts 4.150 keV Det: Octane Elite 25

eZAF Smart Quant Results

Element	Weight %	Atomic %	Net Int.	Error %	Kratio	Z	A	F
C K	0.63	2.79	5.78	26.54	0.0018	1.3151	0.2137	1.0000
O K	0.77	2.57	35.68	11.19	0.0045	1.2653	0.4636	1.0000
MnL	1.72	1.67	35.86	4.36	0.0183	0.9774	1.0882	1.0000
SiK	0.12	0.23	7.04	53.50	0.0007	1.1630	0.4693	1.0029
FeK	96.77	92.74	2942.35	1.59	0.9637	0.9954	1.0001	1.0004

Appendix C. Comprehensive tensile test report

Tensile tests from Beam 2

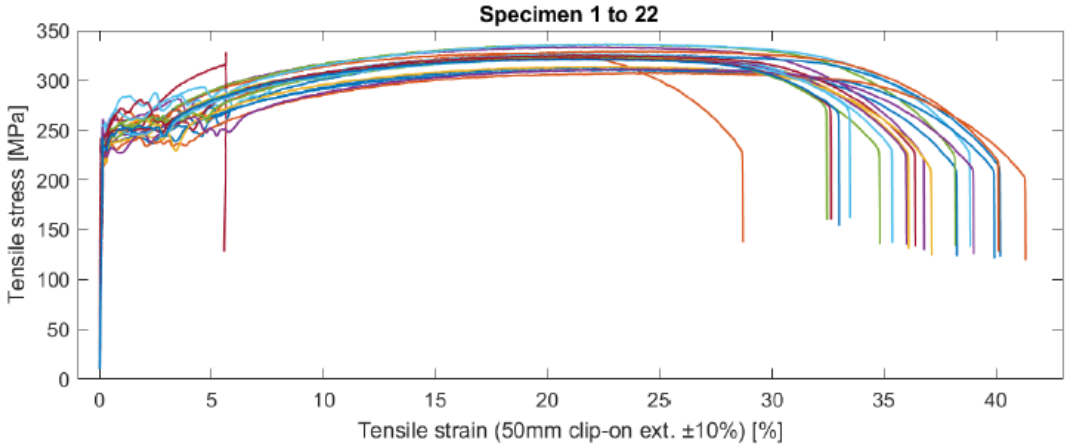

	Specimen label	Location	Modulus (Automatic Young's) [GPa]	Tensile stress at Yield (EN\\ISO lower yield) [MPa]	Tensile stress at Yield (EN\\ISO upper yield) [MPa]	Tensile stress at Yield (Offset 0.2 %) [MPa]	Tensile stress at Tensile strength [MPa]	Tensile stress at Break (Standard) [MPa]	% Elongation at tensile strength at Non-proportional elongation (Standard) [%]	% Elongation at break at Non-proportional elongation (Standard) [%]
5	2,1 B3	2.1 B	199.25	217.51	230.89	221.93	243.91	268.00	2.06	4.44
6	2,1 B2	2.1 B	196.19	226.96	247.00	226.81	326.53	229.15	18.14	28.51
7	2,1 B1	2.1 B	203.06	220.80	232.39	221.56	312.76	211.03	22.81	38.09
8	2,1 T1	2.1 T	188.86	245.35	260.47	245.30	332.83	224.20	21.63	36.59
9	2,1 T2	2.1 T	200.71	229.79	249.18	231.06	335.79	225.28	22.40	38.01
10	2,1 T3	2.1 T	207.25	269.74	284.30	245.00	335.72	228.97	22.80	38.66
1	2.2 B1	2.2 B	885.37	221.95	241.80	228.18	325.74	220.99	5.58	5.59
3	2,2 B3	2.2 B	208.32	229.01	248.74	229.11	325.14	214.33	23.62	40.01
4	2,2 B4	2.2 B	193.55	219.70	242.69	219.70	328.64	219.91	23.89	39.94
2	2.2 H5	2.2 H	181.25	249.65	271.93	246.30	324.57	228.78	21.64	36.20
15	2,2 H1	2.2 H	205.26	-----	-----	232.16	323.77	227.95	21.42	35.91
16	2,2 H2	2.2 H	200.87	225.18	231.92	225.17	322.22	227.63	21.77	35.82
17	2,2 H3	2.2 H	200.31	-----	-----	232.07	322.94	229.82	20.96	34.62
18	2,2 H4	2.2 H	207.07	-----	-----	244.81	325.87	232.00	21.79	35.18

	Specimen label	Location	Modulus (Automatic Young's) [GPa]	Tensile stress at Yield (EN\\ISO lower yield) [MPa]	Tensile stress at Yield (EN\\ISO upper yield) [MPa]	Tensile stress at Yield (Offset 0.2 %) [MPa]	Tensile stress at Tensile strength [MPa]	Tensile stress at Break (Standard) [MPa]	% Elongation at tensile strength at Non-proportional elongation (Standard) [%]	% Elongation at break at Non-proportional elongation (Standard) [%]
19	2,2 T1	2.2 T	206.90	216.12	243.25	217.57	310.25	209.95	22.72	39.77
20	2,2 T2	2.2 T	277.82	-----	-----	219.19	307.21	203.95	24.87	41.17
21	2,2 T3	2.2 T	187.71	216.78	233.31	217.37	313.00	211.76	22.14	36.93
22	2,2 T4	2.2 T	200.03	227.26	253.02	223.29	310.76	211.51	24.06	38.82
11	2,2 V1	2.2 V	196.83	228.82	241.45	229.02	321.14	271.77	21.76	32.23
12	2,2 V2	2.2 V	191.62	228.70	233.32	228.97	320.80	269.80	21.60	33.27
13	2,2 V3	2.2 V	203.09	228.38	236.25	230.02	321.70	272.90	21.31	32.43
14	2,2 V4	2.2 V	196.70	229.86	242.46	229.61	320.72	268.54	21.17	32.77

Appendix D. Impact tests data

Specimen location	Impact strength [Joules]								
	20°C			0°C			- 20°C		
2,1 T	14,4	13,8	17,8	7,5	6,6	7,7	5	6,1	7,1
2,2 T	14,4	12,5	15	7,6	7,7	6,7	5,2	4,9	4,5
2,2 W	10,6	12,9	11,2	6,7	6	6,7	4,2	6,4	5,1
2,2 B	16,5	16,4	11,2	7,5	5,9	7,1	4,9	4,5	4,9

Appendix E. Hardness data

Test location	Number of indentations	Average	SD	Min	Max
2,1 T1	12	96.8	1.75	94.4	99.4
2,1 T3	12	92.9	2.19	89.5	96.8
2,1 W2	70+	98	Lost data	Lost data	Lost data
2,1 W3	12	104.6	2.64	100.3	109.24
2,1 B2	12	92.5	3.99	87.0	97.4
2,1 B4	12	94.2	2.52	90.7	99.3
2,2 T1	12	93.7	2.54	91.1	99.5
2,2 T3	78	92.4	3.03	83.0	99.0
2,2 T5	12	93.3	1.88	90.8	98.0
2,2 W1	12	100.6	1.32	98.0	101.0
2,2 W2	12	99.9	1.84	97.4	103.9
2,2 W3	80	98.5	4.60	89.0	106.0
2,2 B2	12	92.5	2.72	87.7	96.5
2,2 B3	12	97.6	3.04	95.1	105.4
2,2 B5	110	94.1	3.61	87.1	105.0

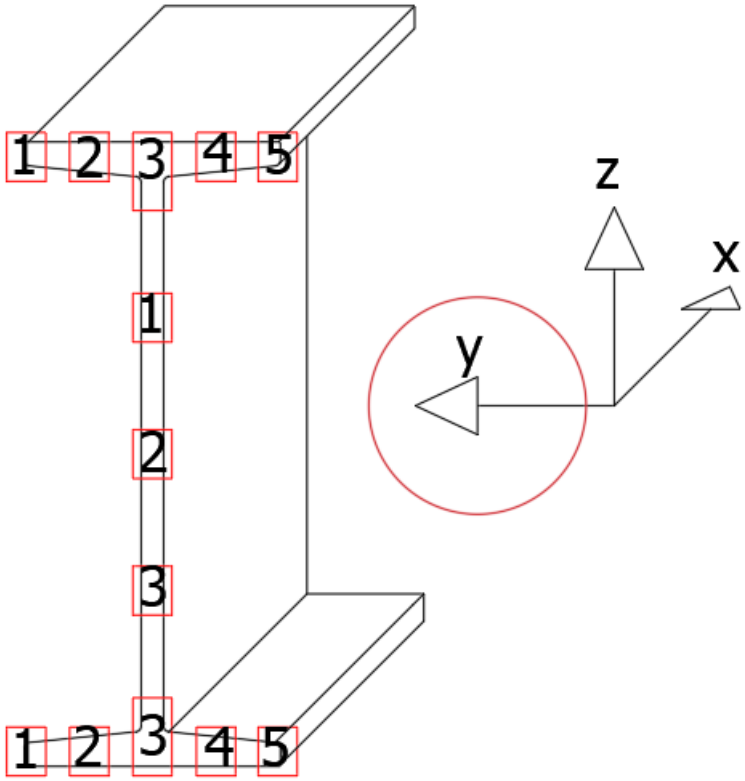

Appendix F. Buckling test report

Toni Technik

Simple standard protocol 15.05.2023

Parameter table:

Test protocol : Per Kristian
Tester :
Creation date : 27.04.2023

Type strain extensometer :
Machine data : Controller TT0322
PistonStroke
LoadCell 400 kN

Results:

Date	ID	a mm	b mm	h mm	F_m kN
28.04.2023	Beam 1, test one	131,0	3250,0	320,0	395,23
28.04.2023	Beam 1, test two	131,0	3250,0	320,0	396,28
15.05.2023	Beam 3	131,0	3300,0	320,0	286,74
15.05.2023	Beam 4	131,0	3340,0	320,0	319,91

Series graphics:

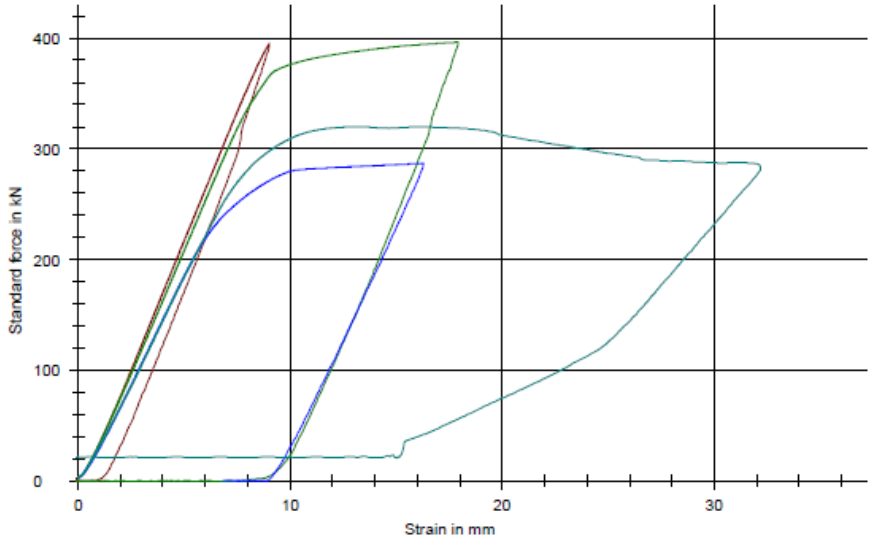

Statistics:

Series n = 4	a mm	b mm	h mm	F_m kN
$\bar{x}$	131,0	3285,0	320,0	349,54
s	0,0	43,6	0,0	55,06
v	0,00	1,33	0,00	15,75

Page 1/1

F.1 SAP2000

Beam 1, test one using material properties from tensile testing:

Job Number _____

Engineer _____

SAP2000

```
 Eurocode 3-2005 STEEL SECTION CHECK    (Summary for Combo and Station)
 Units  :  KN, m, C

 Frame :  10       X Mid:  1,675     Combo:  Applied Comb    Design Type:  Beam
 Length:  2,55     Y Mid:  0,        Shape:  bridge cross secFrame Type:  DCH-MRF
 Loc   :  2,55     Z Mid:  0,        Class:  Class 3         Rolled : No

 Country=Norway                      Combination=Eq. 6.10
Reliability=Class 2
 Interaction=Method 2 (Annex B)      MultiResponse=Envelopes              P-Delta Done?
No
 Consider Torsion? No

 GammaM0=1,05      GammaM1=1,05      GammaM2=1,25
 An/Ag=1,          RLLF=1,           PLLF=0,75         D/C Lim=0,95       Prin. Axis
Angle = 0, deg

 Aeff=0,007        Av,2=0,004        Av,3=0,004        eNy=0,             eNz=0,
 A=0,007           Iy=1,160E-04      iy=0,126          Wel,y=7,238E-04    Weff,y=
7,238E-04
 It=4,934E-07      Iz=5,178E-06      iz=0,027          Wel,z=7,905E-05    Weff,z=
7,905E-05
 Iw=0,             Iyz=0,            h=0,321           Wpl,y=8,487E-04
 E=188000000,      fy=211000,        fu=311,           Wpl,z=1,321E-04



 STRESS CHECK FORCES & MOMENTS
     Location          Ned       My,Ed       Mz,Ed       V2,Ed       V3,Ed          TEd
     2,55                0,      21,137          0,      19,216          0,           0,

 PMM DEMAND/CAPACITY RATIO   (Governing Equation EC3 6.3.3(4)-6.62)
     D/C Ratio:    0,152 = 0, + 0,152 + 0,    <          0,95          OK
                     = NEd/(Chi_z NRk/GammaM1) + kzy (My,Ed+NEd eNy)/(Chi_LT
My,Rk/GammaM1)
                       + kzz (Mz,Ed+NEd eNz)/(Mz,Rk/GammaM1)       (EC3
6.3.3(4)-6.62)

 AXIAL FORCE DESIGN
                          NEd       Nc,Rd       Nt,Rd
                       Force    Capacity    Capacity
     Axial                0,    1471,171       1,639

                      Npl,Rd       Nu,Rd       Ncr,T      Ncr,TF       An/Ag
                   1471,171       1,639    2155,042    1477,407          1,

                Curve   Alpha         Ncr   LambdaBar         Phi         Chi       Nb,Rd
     Y-Y            c    0,49   33103,451       0,216       0,527       0,992    1459,163
     Y-Y Braced     c    0,49   33103,451       0,216       0,527       0,992    1459,163
     Z-Z            c    0,49    1477,407       1,023       1,224       0,527     775,272
     Z-Z Braced     c    0,49    1477,407       1,023       1,224       0,527     775,272
     Torsional TF   c    0,49    1477,407       1,023       1,224       0,527     775,272

 MOMENT DESIGN
                          MEd    MEd,span       Mc,Rd       Mv,Rd       Mn,Rd       Mb,Rd
                       Moment      Moment    Capacity    Capacity    Capacity    Capacity
     Y-Y                  0,      21,137     145,451     145,451     145,451     139,152
     Z-Z                  0,          0,      15,885      15,885      15,885

                Curve AlphaLT LambdaBarLT       PhiLT       ChiLT          Iw         Mcr
     LTB            d    0,76       0,256       0,554       0,957          0,    2333,349

     Factors      kw          C1          C2          C3
                   1,       1,046       0,43        1,12
                   za          zs          zg          zz          zj
                -1,737          0,      -1,737  -1,475E-15   1,475E-15

                             kyy         kyz         kzy         kzz
     Factors                 0,9          1,          1,          1,
```

Beam 1, test one using material properties from S235:

SAP2000 Engineer _____

Eurocode 3-2005 STEEL SECTION CHECK (Summary for Combo and Station)
Units : KN, m, C

Frame : 10 X Mid: 1,675 Combo: Applied Comb Design Type: Beam
Length: 2,55 Y Mid: 0, Shape: bridge cross secFrame Type: DCH-MRF
Loc : 2,55 Z Mid: 0, Class: Class 3 Rolled : No

Country=Norway Combination=Eq. 6.10
Reliability=Class 2
Interaction-Method 2 (Annex B) MultiResponse=Envelopes P-Delta Done?
No
Consider Torsion? No

GammaM0=1,05 GammaM1=1,05 GammaM2=1,25
An/Ag=1, RLLF=1, PLLF=0,75 D/C Lim=0,95 Prin. Axis
Angle = 0, deg

Aeff=0,007 Av,2=0,003 Av,3=0,004 eNy=0, eNz=0,
A=0,007 Iy=1,039E-04 iy=0,126 Wel,y=6,480E-04 Weff,y=
6,480E-04
It=4,417E-07 Iz=4,635E-06 iz=0,027 Wel,z=7,077E-05 Weff,z=
7,077E-05
Iw=0, Iyz=0, h=0,321 Wpl,y=7,621E-04
E=210000000, fy=235000, fu=370000, Wpl,z=1,186E-04

STRESS CHECK FORCES & MOMENTS

Location	Ned	My,Ed	Mz,Ed	V2,Ed	V3,Ed	TEd
2,55	0,	21,137	0,	19,216	0,	0,

PMM DEMAND/CAPACITY RATIO (Governing Equation EC3 6.3.3(4)-6.62)
D/C Ratio: 0,152 = 0, + 0,152 + 0, < 0,95 OK
= NEd/(Chi_z NRk/GammaM1) + kzy (My,Ed+NEd eNy)/(Chi_LT
My,Rk/GammaM1)
+ kzz (Mz,Ed+NEd eNz)/(Mz,Rk/GammaM1) (EC3
6.3.3(4)-6.62)

AXIAL FORCE DESIGN

	NEd Force	Nc,Rd Capacity	Nt,Rd Capacity
Axial	0,	1466,855	1466,855

Npl,Rd	Nu,Rd	Ncr,T	Ncr,TF	An/Ag
1466,855	1745,995	2155,042	1477,407	1,

	Curve	Alpha	Ncr	LambdaBar	Phi	Chi	Nb,Rd
Y-Y	c	0,49	33103,451	0,216	0,527	0,992	1455,119
Y-Y Braced	c	0,49	33103,451	0,216	0,527	0,992	1455,119
Z-Z	c	0,49	1477,407	1,021	1,222	0,528	774,254
Z-Z Braced	c	0,49	1477,407	1,021	1,222	0,528	774,254
Torsional TF	c	0,49	1477,407	1,021	1,222	0,528	774,254

MOMENT DESIGN

	MEd Moment	MEd,span Moment	Mc,Rd Capacity	Mv,Rd Capacity	Mn,Rd Capacity	Mb,Rd Capacity
Y-Y	0,	21,137	145,025	145,025	145,025	138,785
Z-Z	0,	0,	15,838	15,838	15,838	

	Curve	AlphaLT	LambdaBarLT	PhiLT	ChiLT	Iw	Mcr
LTB	d	0,76	0,255	0,554	0,957	0,	2333,349

	kw	C1	C2	C3		
Factors	1,	1,046	0,43	1,12		
	za	zs	zg	zz	zj	
	-1,737	0,	-1,737	-1,475E-15	1,475E-15	

	kyy	kyz	kzy	kzz
Factors	0,9	1,	1,	1,

Beam 1, test two using material properties from tensile testing:

SAP2000

Job Number _____
Engineer _____

```
 Eurocode 3-2005 STEEL SECTION CHECK     (Summary for Combo and Station)
 Units  :  KN, m, C

 Frame :  10       X Mid:  1,675     Combo:  Applied Comb    Design Type:  Beam
 Length:  2,55     Y Mid:  0,        Shape:  bridge cross secFrame Type:  DCH-MRF
 Loc   :  2,55     Z Mid:  0,        Class:  Class 3         Rolled : No

 Country=Norway                      Combination=Eq. 6.10
Reliability=Class 2
 Interaction=Method 2 (Annex B)      MultiResponse=Envelopes              P-Delta Done?
No
 Consider Torsion? No

 GammaM0=1,05      GammaM1=1,05      GammaM2=1,25
 An/Ag=1,          RLLF=1,           PLLF=0,75         D/C Lim=0,95       Prin. Axis
Angle = 0, deg

 Aeff=0,007        Av,2=0,004        Av,3=0,004        eNy=0,             eNz=0,
 A=0,007           Iy=1,160E-04      iy=0,126          Wel,y=7,238E-04    Weff,y=
7,238E-04
 It=4,934E-07      Iz=5,178E-06      iz=0,027          Wel,z=7,905E-05    Weff,z=
7,905E-05
 Iw=0,             Iyz=0,            h=0,321           Wpl,y=8,487E-04
 E=188000000,      fy=211000,        fu=311,           Wpl,z=1,321E-04



 STRESS CHECK FORCES & MOMENTS
     Location          Ned       My,Ed       Mz,Ed       V2,Ed       V3,Ed          TEd
     2,55               0,      23,827          0,      19,216          0,           0,

 PMM DEMAND/CAPACITY RATIO   (Governing Equation EC3 6.3.3(4)-6.62)
     D/C Ratio:    0,171 = 0, + 0,171 + 0,    <          0,95          OK
                       = NEd/(Chi_z NRk/GammaM1) + kzy (My,Ed+NEd eNy)/(Chi_LT
My,Rk/GammaM1)
                         + kzz (Mz,Ed+NEd eNz)/(Mz,Rk/GammaM1)        (EC3
6.3.3(4)-6.62)

 AXIAL FORCE DESIGN
                          NEd       Nc,Rd       Nt,Rd
                       Force    Capacity    Capacity
     Axial               0,    1471,171       1,639

                       Npl,Rd       Nu,Rd       Ncr,T      Ncr,TF       An/Ag
                    1471,171       1,639    2155,042    1477,407          1,

                 Curve   Alpha         Ncr   LambdaBar         Phi         Chi       Nb,Rd
     Y-Y             c    0,49   33103,451       0,216       0,527       0,992    1459,163
     Y-Y Braced      c    0,49   33103,451       0,216       0,527       0,992    1459,163
     Z-Z             c    0,49    1477,407       1,023       1,224       0,527     775,272
     Z-Z Braced      c    0,49    1477,407       1,023       1,224       0,527     775,272
     Torsional TF    c    0,49    1477,407       1,023       1,224       0,527     775,272

 MOMENT DESIGN
                          MEd    MEd,span       Mc,Rd       Mv,Rd       Mn,Rd       Mb,Rd
                      Moment      Moment    Capacity    Capacity    Capacity    Capacity
     Y-Y                 0,      23,827     145,451     145,451     145,451     139,152
     Z-Z                 0,           0,     15,885      15,885      15,885

                 Curve AlphaLT LambdaBarLT       PhiLT       ChiLT          Iw         Mcr
     LTB             d    0,76       0,256       0,554       0,957          0,   2333,349

     Factors       kw        C1          C2          C3
                    1,    1,046        0,43        1,12
                    za        zs          zg          zz          zj
                -1,737        0,      -1,737  -1,475E-15   1,475E-15

                          kyy         kyz         kzy         kzz
     Factors              0,9          1,          1,          1,
```

Beam 1, test two using material properties from S235:

SAP2000 Engineer _____

```
 Eurocode 3-2005 STEEL SECTION CHECK    (Summary for Combo and Station)
 Units  :  KN, m, C

 Frame :  10       X Mid:  1,675     Combo:  Applied Comb    Design Type:  Beam
 Length:  2,55     Y Mid:  0,        Shape:  bridge cross secFrame Type:  DCH-MRF
 Loc   :  2,55     Z Mid:  0,        Class:  Class 3         Rolled : No

 Country=Norway                      Combination=Eq. 6.10
Reliability=Class 2
 Interaction=Method 2 (Annex B)      MultiResponse=Envelopes              P-Delta Done?
No
 Consider Torsion? No

 GammaM0=1,05      GammaM1=1,05      GammaM2=1,25
 An/Ag=1,          RLLF=1,           PLLF=0,75         D/C Lim=0,95       Prin. Axis
Angle = 0, deg

 Aeff=0,007        Av,2=0,003        Av,3=0,004        eNy=0,             eNz=0,
 A=0,007           Iy=1,039E-04      iy=0,126          Wel,y=6,480E-04    Weff,y=
6,480E-04
 It=4,417E-07      Iz=4,635E-06      iz=0,027          Wel,z=7,077E-05    Weff,z=
7,077E-05
 Iw=0,             Iyz=0,            h=0,321           Wpl,y=7,621E-04
 E=210000000,      fy=235000,        fu=370000,        Wpl,z=1,186E-04


 STRESS CHECK FORCES & MOMENTS
     Location            Ned       My,Ed       Mz,Ed       V2,Ed       V3,Ed          TEd
     2,55                  0,      23,827          0,      19,216          0,           0,

 PMM DEMAND/CAPACITY RATIO    (Governing Equation EC3 6.3.3(4)-6.62)
     D/C Ratio:    0,172 = 0, + 0,172 + 0,    <          0,95          OK
                     = NEd/(Chi_z NRk/GammaM1) + kzy (My,Ed+NEd eNy)/(Chi_LT
My,Rk/GammaM1)
                       + kzz (Mz,Ed+NEd eNz)/(Mz,Rk/GammaM1)        (EC3
6.3.3(4)-6.62)

 AXIAL FORCE DESIGN
                          NEd       Nc,Rd       Nt,Rd
                       Force    Capacity    Capacity
     Axial                 0,    1466,855    1466,855

                       Npl,Rd       Nu,Rd       Ncr,T      Ncr,TF       An/Ag
                    1466,855    1745,995    2155,042    1477,407          1,

                Curve   Alpha         Ncr   LambdaBar         Phi         Chi       Nb,Rd
     Y-Y            c    0,49    33103,451       0,216       0,527       0,992    1455,119
     Y-Y Braced     c    0,49    33103,451       0,216       0,527       0,992    1455,119
     Z-Z            c    0,49    1477,407        1,021       1,222       0,528     774,254
     Z-Z Braced     c    0,49    1477,407        1,021       1,222       0,528     774,254
     Torsional TF   c    0,49    1477,407        1,021       1,222       0,528     774,254

 MOMENT DESIGN
                          MEd    MEd,span       Mc,Rd       Mv,Rd       Mn,Rd       Mb,Rd
                      Moment      Moment    Capacity    Capacity    Capacity    Capacity
     Y-Y                   0,      23,827     145,025     145,025     145,025     138,785
     Z-Z                   0,           0,     15,838      15,838      15,838

                Curve AlphaLT LambdaBarLT       PhiLT       ChiLT          Iw         Mcr
     LTB            d    0,76       0,255       0,554       0,957          0,    2333,349

     Factors       kw        C1          C2          C3
                    1,     1,046       0,43        1,12
                    za        zs          zg          zz          zj
                -1,737        0,      -1,737  -1,475E-15   1,475E-15

                          kyy         kyz         kzy         kzz
     Factors              0,9          1,          1,          1,
```

Beam 3 and 4 using material properties from tensile testing:

SAP2000 Engineer _____

```
 Eurocode 3-2005 STEEL SECTION CHECK    (Summary for Combo and Station)
 Units  :  KN, m, C

 Frame :  10       X Mid:  1,675     Combo:  Applied Comb    Design Type:  Beam
 Length:  2,55     Y Mid:  0,        Shape:  bridge cross secFrame Type:  DCH-MRF
 Loc   :  2,55     Z Mid:  0,        Class:  Class 3         Rolled : No

 Country=Norway                     Combination=Eq. 6.10
Reliability=Class 2
 Interaction=Method 2 (Annex B)     MultiResponse=Envelopes              P-Delta Done?
No
 Consider Torsion? No

 GammaM0=1,05      GammaM1=1,05     GammaM2=1,25
 An/Ag=1,          RLLF=1,          PLLF=0,75         D/C Lim=0,95       Prin. Axis
Angle = 0, deg

 Aeff=0,007        Av,2=0,004       Av,3=0,004        eNy=0,             eNz=0,
 A=0,007           Iy=1,160E-04     iy=0,126          Wel,y=7,238E-04    Weff,y=
7,238E-04
 It=4,934E-07      Iz=5,178E-06     iz=0,027          Wel,z=7,905E-05    Weff,z=
7,905E-05
 Iw=0,             Iyz=0,           h=0,321           Wpl,y=8,487E-04
 E=188000000,      fy=211000,       fu=311,           Wpl,z=1,321E-04



 STRESS CHECK FORCES & MOMENTS
    Location          Ned       My,Ed       Mz,Ed       V2,Ed       V3,Ed         TEd
    2,55                0,       12,73         0,       9,608         0,          0,

 PMM DEMAND/CAPACITY RATIO   (Governing Equation EC3 6.3.3(4)-6.62)
    D/C Ratio:    0,088 = 0, + 0,088 + 0,    <         0,95          OK
                  = NEd/(Chi_z NRk/GammaM1) + kzy (My,Ed+NEd eNy)/(Chi_LT
My,Rk/GammaM1)
                    + kzz (Mz,Ed+NEd eNz)/(Mz,Rk/GammaM1)       (EC3
6.3.3(4)-6.62)

 AXIAL FORCE DESIGN
                        NEd       Nc,Rd       Nt,Rd
                     Force     Capacity    Capacity
    Axial              0,     1471,171       1,639

                    Npl,Rd       Nu,Rd       Ncr,T      Ncr,TF       An/Ag
                  1471,171       1,639    2155,042    1477,407          1,

              Curve   Alpha         Ncr   LambdaBar         Phi         Chi       Nb,Rd
    Y-Y           c    0,49   33103,451       0,216       0,527       0,992    1459,163
    Y-Y Braced    c    0,49   33103,451       0,216       0,527       0,992    1459,163
    Z-Z           c    0,49    1477,407       1,023       1,224       0,527     775,272
    Z-Z Braced    c    0,49    1477,407       1,023       1,224       0,527     775,272
    Torsional TF  c    0,49    1477,407       1,023       1,224       0,527     775,272

 MOMENT DESIGN
                        MEd    MEd,span       Mc,Rd       Mv,Rd       Mn,Rd       Mb,Rd
                    Moment      Moment    Capacity    Capacity    Capacity    Capacity
    Y-Y                0,       12,73     145,451     145,451     145,451     145,451
    Z-Z                0,          0,      15,885      15,885      15,885

              Curve AlphaLT LambdaBarLT       PhiLT       ChiLT          Iw         Mcr
    LTB           d    0,76       0,198       0,519           1,          0,   3899,659

    Factors       kw       C1          C2          C3
                   1,    1,365       0,553       1,73
                   za       zs          zg          zz          zj
               -1,737       0,      -1,737  -1,475E-15   1,475E-15

                         kyy         kyz         kzy         kzz
    Factors              0,9           1,          1,          1,
```

Beam 3 and 4 using material properties from S235:

SAP2000 Engineer _____

Eurocode 3-2005 STEEL SECTION CHECK (Summary for Combo and Station)
Units : KN, m, C

Frame : 10 X Mid: 1,675 Combo: Applied Comb Design Type: Beam
Length: 2,55 Y Mid: 0, Shape: bridge cross secFrame Type: DCH-MRF
Loc : 2,55 Z Mid: 0, Class: Class 3 Rolled : No

Country=Norway Combination=Eq. 6.10
Reliability=Class 2
Interaction=Method 2 (Annex B) MultiResponse=Envelopes P-Delta Done?
No
Consider Torsion? No

GammaM0=1,05 GammaM1=1,05 GammaM2=1,25
An/Ag=1, RLLF=1, PLLF=0,75 D/C Lim=0,95 Prin. Axis
Angle = 0, deg

Aeff=0,007 Av,2=0,003 Av,3=0,004 eNy=0, eNz=0,
A=0,007 Iy=1,039E-04 iy=0,126 Wel,y=6,480E-04 Weff,y=
6,480E-04
It=4,417E-07 Iz=4,635E-06 iz=0,027 Wel,z=7,077E-05 Weff,z=
7,077E-05
Iw=0, Iyz=0, h=0,321 Wpl,y=7,621E-04
E=210000000, fy=235000, fu=370000, Wpl,z=1,186E-04

STRESS CHECK FORCES & MOMENTS

Location	Ned	My,Ed	Mz,Ed	V2,Ed	V3,Ed	TEd
2,55	0,	12,73	0,	9,608	0,	0,

PMM DEMAND/CAPACITY RATIO (Governing Equation EC3 6.3.3(4)-6.62)
D/C Ratio: 0,088 = 0, + 0,088 + 0, < 0,95 OK
= NEd/(Chi_z NRk/GammaM1) + kzy (My,Ed+NEd eNy)/(Chi_LT
My,Rk/GammaM1)
+ kzz (Mz,Ed+NEd eNz)/(Mz,Rk/GammaM1) (EC3
6.3.3(4)-6.62)

AXIAL FORCE DESIGN

	NEd Force	Nc,Rd Capacity	Nt,Rd Capacity
Axial	0,	1466,855	1466,855

Npl,Rd	Nu,Rd	Ncr,T	Ncr,TF	An/Ag
1466,855	1745,995	2155,042	1477,407	1,

	Curve	Alpha	Ncr	LambdaBar	Phi	Chi	Nb,Rd
Y-Y	c	0,49	33103,451	0,216	0,527	0,992	1455,119
Y-Y Braced	c	0,49	33103,451	0,216	0,527	0,992	1455,119
Z-Z	c	0,49	1477,407	1,021	1,222	0,528	774,254
Z-Z Braced	c	0,49	1477,407	1,021	1,222	0,528	774,254
Torsional TF	c	0,49	1477,407	1,021	1,222	0,528	774,254

MOMENT DESIGN

	MEd Moment	MEd,span Moment	Mc,Rd Capacity	Mv,Rd Capacity	Mn,Rd Capacity	Mb,Rd Capacity
Y-Y	0,	12,73	145,025	145,025	145,025	145,025
Z-Z	0,	0,	15,838	15,838	15,838	

	Curve	AlphaLT	LambdaBarLT	PhiLT	ChiLT	Iw	Mcr
LTB	d	0,76	0,198	0,519	1,	0,	3899,659

Factors	kw	C1	C2	C3
	1,	1,365	0,553	1,73

za	zs	zg	zz	zj
-1,737	0,	-1,737	-1,475E-15	1,475E-15

	kyy	kyz	kzy	kzz
Factors	0,9	1,	1,	1,